ORIGINAL ARTICLE

The intracellular ROS accumulation in elicitor-induced immunity requires the multiple organelle-targeted Arabidopsis NPK1-related protein kinases

Lucia Marti[1] | Daniel-Valentin Savatin[1] | Nora Gigli-Bisceglia[1] |
Valeria de Turris[2] | Felice Cervone[1] | Giulia De Lorenzo[1]

[1]Department of Biology and Biotechnology "Charles Darwin", Sapienza University, Rome, Italy

[2]Italian Institute of Technology, Rome, Italy

Correspondence
Daniel Valentin Savatin, Department of Agriculture and Forest Sciences, Tuscia University, Via San Camillo de Lellis snc, 01100, Viterbo, Italy.
Email: daniel.savatin@unitus.it

Present address
Daniel V. Savatin, Department of Agriculture and Forest Sciences, Tuscia University, Viterbo, Italy.Present address Nora Gigli-Bisceglia, Laboratory of Plant Physiology, Wageningen University and Research, Wageningen, the Netherlands.

Abstract

Recognition at the plasma membrane of danger signals (elicitors) belonging to the classes of the microbe/pathogen- and damage-associated molecular patterns is a key event in pathogen sensing by plants and is associated with a rapid activation of immune responses. Different cellular compartments, including plasma membrane, chloroplasts, nuclei and mitochondria, are involved in the immune cellular program. However, how pathogen sensing is transmitted throughout the cell remains largely to be uncovered. Arabidopsis NPK1-related Proteins (ANPs) are mitogen-activated protein kinase kinase kinases previously shown to have a role in immunity. In this article, we studied the in vivo intracellular dynamics of ANP1- and ANP3-GFP fusions and found that under basal physiological conditions both proteins are present in the cytosol, while ANP3 is also localized in mitochondria. After elicitor perception, both proteins are present also in the plastids and nuclei, revealing a localization pattern that is so far unique. The N-terminal region of the protein kinases is responsible for their localization in mitochondria and plastids. Moreover, we found that the localization of ANPs coincides with the sites of elicitor-induced ROS accumulation and that plants lacking ANP function do not accumulate intracellular ROS.

KEYWORDS
danger signaling, innate immunity, kinases, oligogalacturonides, ROS production, subcellular localization

1 | INTRODUCTION

Due to their sessile conditions plants must resist to continuous attacks by microbial pathogens and they succeed because of a powerful immune system. Plant immunity is activated by plasma membrane localized Pattern Recognition Receptors (PRRs) capable of sensing the presence of conserved Microbe/Pathogen-Associated Molecular Patterns (MAMPs/PAMPs) as non-self molecules, and activating the so-called PAMP-triggered immunity (PTI) (Boller & He, 2009; Saijo, Loo, & Yasuda, 2018). Representative MAMPs are the bacterial

peptides elf18 and flg22, derived from the bacterial elongation factor EF-Tu and flagellin, respectively, that are recognized by the transmembrane leucine-rich repeat receptor kinases (RK) EF-TU RECEPTOR (EFR) and FLAGELLIN-SENSING 2 (FLS2) (Gómez-Gómez & Boller, 2000; Zipfel et al., 2006). Endogenous molecules released during infection, for instance when the cell wall is degraded by microbial enzymes or upon mechanical wounding (Bellincampi, Cervone, & Lionetti, 2014; Savatin, Gramegna, Modesti, & Cervone, 2014b), are referred to as Damage-Associated Molecular Patterns (DAMPs). DAMPs are also recognized by PRRs as danger signals and contribute to the activation of the plant immune response (Gust, Pruitt, & Nürnberger, 2017; Schwessinger & Ronald, 2012). Well characterized

DAMPs are the oligogalacturonides (OGs) formed by ten to about sixteen α-1,4-D-galactopyranosyluronic acid (GalA) residues released upon fragmentation of the plant cell wall homogalacturonan (De Lorenzo, Ferrari, Cervone, & Okun, 2018; Ferrari et al., 2013). Recent findings suggest that perception of OGs requires more than one transmembrane receptor complex (Gravino et al., 2017) and, so far, only the WALL-ASSOCIATED KINASE 1 (WAK1), a RK containing epidermal-growth factor-like repeats has been characterized as an OG receptor (Brutus, Sicilia, Macone, Cervone, & De Lorenzo, 2010).

The recognition of DAMPs or MAMPs through PRRs activates downstream signaling pathways leading to rapid defence-related responses such as production of reactive oxygen species (ROS), changes in ion fluxes and induction of defense gene expression, as well as late responses such as callose deposition, growth inhibition and protection against further pathogen attacks (Couto & Zipfel, 2016; Ferrari et al., 2013). In plants, like in animals, immune signaling occurs through dynamic, complex and cross-talking transduction pathways that include phosphorylation cascades of mitogen-activated protein kinases (MAPKs) (Suarez Rodriguez, Petersen, & Mundy, 2010). A MAPK cascade consists of a core module of three kinases that perform sequential phosphorylation reactions: a MAP kinase kinase kinase (MAPKKK, also called MAP3K) activates by phosphorylation a MAP kinase kinase (MAPKK or MAP2K), which activates a MAP kinase (MAPK or MAPK). Sixty putative MAPKKKs, 10 MAPKKs and 20 MAPKs are encoded by the Arabidopsis genome (Colcombet & Hirt, 2008) leading to a complexity that hinders the characterization of this transduction system.

Different MAP kinase modules have been shown to be involved in Arabidopsis immunity (Kong et al., 2012; Meng & Zhang, 2013; Suarez Rodriguez et al., 2010; Xu & Zhang, 2015; Zhang, Su, Zhang, Xu, & Zhang, 2018). Among the MAPK elements, the Arabidopsis MAPKKK and MPK6 are phosphorylated within minutes upon elicitation with OGs or flg22 (Galletti, Ferrari, & De Lorenzo, 2011; Savatin et al., 2014a). MPK6 is required for full elicitor-induced up-regulation of defense genes and protection against *B. cinerea* (Galletti et al., 2011; Savatin, Gigli-Bisceglia, et al., 2014a). MPK3 and MPK6 are activated by cold, hormones and H_2O_2 (Xing, Jia, & Zhang, 2009) and, along with MPK4, participate as part of different MAPK modules in the activation of the signaling pathway triggered by a large variety of stimuli in both immunity [MEKK1-MKK4/5-MPK3/6, MEKK1-MKK1/2-MPK4] and development [YODA-MKK4/5-MPK3/6] (Zhang et al., 2018).

Among the MAPKKK families identified so far, the ARABIDOPSIS NPK1-RELATED PROTEIN KINASE (ANP) family, which comprises three members and was initially identified for its homology with the tobacco *NUCLEUS- AND PHRAGMOPLAST-LOCALIZED KINASES 1* (*NPK1*) gene (Jouannic et al., 1999; Sasabe & Machida, 2012), has been shown to play a role in the activation of MPK3 and MPK6 in response to H_2O_2 (Kovtun, Chiu, Tena, & Sheen, 2000; Savatin, Gigli-Bisceglia, et al., 2014a). ANPs are also essential for plant development, since no triple mutant could be obtained by crossings (Krysan, Jester, Gottwald, & Sussman, 2002). In the *anp2 anp3* double mutant, cytokinesis is defective, a feature that has been associated with a defective organization of cortical microtubules (Beck, Komis, Ziemann, Menzel, &

Samaj, 2011). Morphological and cytokinesis defects similar to those of *anp2 anp3* double mutants are observed in loss-of-function mutants in the module MEKK1-MPK4 (Su et al., 2013) and are mediated by an accumulation of transcripts of the MAPKKK *MEKK2*. Increased abundance of these transcripts indicates a disruption of the integrity of the MAPK module that is sensed by the nucleotide-binding-leucine-rich repeat protein SUMM2, leading to a SA-dependent autoimmune response (Zhang et al., 2017).

It is noteworthy that, when compared to *anp2 anp3*, the *anp1 anp3* double mutant shows more moderate defects, whereas *anp1 anp2* is phenotypically normal, hinting that ANPs are functionally redundant but contribute to development to differing extents. Indeed, differences among ANP1 and ANP3 have been described as regards the activation of MKK6 during cytokinesis (Takahashi, Soyano, Kosetsu, Sasabe, & Machida, 2010). Cytokinesis and developmental defects become more evident in conditional *anp* triple mutants (hereon indicated as triple mutants) generated by individually expressing *ANP1-* and *ANP3*-specific artificial microRNAs (amiRNAs) under the control of a β-estradiol-inducible promoter, respectively, in *anp2 anp3* (amiR1 plants) and *anp1 anp2* (amiR3 plants) double mutant background (Savatin, Gigli-Bisceglia, et al., 2014a). The *anp2 anp3* mutant and the triple mutants show enhanced basal levels of stress-related genes that is independent of an increased expression of *MEKK2* (Savatin, Gigli-Bisceglia, et al., 2014a), and, at least in the double *anp2 anp3*, also independent of SUMM2, requiring instead the defense regulators PAD4 and EDS1 (Lian et al., 2018).

Characterization of the conditional triple mutants has shown that ANPs are required for several OG-induced responses, such as mediating extracellular ROS accumulation catalyzed by the NADPH oxidase RBOHD, MPK3/6 phosphorylation, induction of defense gene expression, and protection against *B.cinerea* (Savatin, Gigli-Bisceglia, et al., 2014a). Moreover, their loss affects cell wall composition and leads to typical cell wall damage-induced phenotypes, such as ectopic lignification and jasmonic acid accumulation (Gigli-Bisceglia, Savatin, Cervone, Engelsdorf, & De Lorenzo, 2018).

In this work, we investigated the subcellular localization of ANPs and their dynamics during elicitor-induced immunity. We report that, in response to OGs and elf18, ANPs localize in mitochondria, plastids and nuclei, organelles that are sites of accumulation of ROS triggered by these elicitors. By using the conditional triple *anp* mutants, we also show that ANPs are required for ROS accumulation in these organelles, supporting the hypothesis of an important role of ANPs in the regulation of the oxidative burst also in intracellular compartments. Here, we envision a signal transduction dynamic that is so far unique in plant cell biology and points to ANPs as important regulators of plant immunity.

2 | MATERIAL AND METHODS

2.1 | Plant growth and treatment

Arabidopsis (*Arabidopsis thaliana*) Columbia-0 (Col-0) and Wassilewskija (Ws) wild-type seeds were purchased from Lehle Seeds. The generation

of the conditional *anp* triple mutant through the expression of β-estradiol-inducible artificial microRNAs (amiRNA) having *ANP1* transcripts as specific targets in *anp2 anp3* double KO mutant, kindly provided by Patrick J. Krysan (Department of Horticulture, University of Wisconsin), [amiR1 lines (#2.5 and #8.7) in Ws background] has been previously described (Savatin et al., 2014a). Briefly, the amiRNA was designed using a Web-based tool (http://wmd.weigelworld.org). The primary amiRNA was obtained as previously described (Schwab et al., 2006) and inserted in the pMDC7 binary vector downstream of a β-estradiol-inducible promoter (Curtis and Grossniklaus, 2003) by using the Gateway Recombination Cloning Technology (Life Technologies).

For transcript analyses, seedlings were grown in sterile 0.5 MS supplemented with 0.5% sucrose pH 5.7 for 10 days in plastic multiwells (10 seedlings/well) at 22°C and 70% relative humidity under a 16 hr/8 hr light/dark cycle (approximately 120 μmol/m^2/s).

OGs with an average DP of 10 to 16, as assessed by matrix-assisted laser desorption/ionization time-of-flight MS, were prepared as previously described (Bellincampi et al., 2000). The elf18 peptide was obtained from EZBiolab (http://www.ezbiolab.com/). OGs and elf18 were used at 100 μg/mL or 100 nM, respectively, unless otherwise indicated. Cycloheximide (CHX; dissolved in DMSO and diluited in MS/2) (Sigma-Aldrich C4859) treatment was performed alone (100 μM final concentration) or in combination with OGs or elf18 on flask-grown seedlings. Pretreatment with the proteasome inhibitor MG132 (Sigma-Aldrich, M7449) was performed overnight on flask-grown seedlings at a final concentration of 10 μM.

2.2 | Generation of transgenic plants

ANP1 and *ANP3* full-length cDNA clones were obtained from Riken BioResource Center (http://www.brc.riken.jp/lab/epd/). Constructs for expression of fluorescent full length ANPs, 68aaANP1NT-GFP, 67aaANP3NT-GFP, ANP lacking the N-terminal part were obtained through the Multisite Gateway Recombination Cloning Technology (Life Technologies) by using the pEN-R2-F-L3 and pEN-L4-2-R1 entry vectors, which contain the GFP coding sequence and the 35S promoter, respectively, and pB7m34GW as destination binary vector, which confers resistance to phosphinothricin. For the construct carrying the GFP alone, the pH7m24GW binary vector, which contains the 35S promoter and confers resistance to hygromicin, was used as a destination vector. For testing the functionality of the ANP-GFP fusions by phenotype rescue, the *P35S:ANP-GFP* cassettes was cloned into the same vector, pH7m24GW. Recombinant plasmids containing either GFP alone or the *P35S:ANP-GFP* cassettes were used to transform the *anp2 anp3* mutant (phosphinothricin- and kanamycin-resistant) by Agrobacterium mediated transformation.

Lines showing levels of ANP-GFP transcripts similar to those of the GFP were selected (Figure S1A).

All Gateway compatible vectors were previously described (Karimi, Inze, & Depicker, 2002) and obtained from Plant Systems Biology (Ghent University; http://gateway.psb.ugent.be/).

For each construct, at least 13 independent transgenic T1 plants (in Col-0 or *anp2 anp3* mutant background) were selected that showed fluorescence in seedling cotyledon cells, as determined by laser-scanning confocal microscopy (LSCM), and two homozygous T3 lines carrying a single insertion were chosen (lines # 38.1 and # 24.1 for P35S:ANP1-GFP, # 4.9 and # 8.1 for *P35S:ANP3-GFP*, # 1.1 and # 2.1 for the control construct *P35S:GFP*. # 1.1 and # 2.2 for the *anp2 anp3/P35S:ANP3-GFP* rescued lines and # 4.1 and #5.1 for *anp2 anp3*/P35S:GFP, respectively).

Arabidopsis plants were transformed by the floral dip method (Clough & Bent, 1998), and transformants were selected on MS half strength medium with phosphinothricin (Basta; final concentration 20 μg/mL), or hygromicin (Hyg; final concentration 25 μg/mL) and 0.7% (w/v) agar.

T3 lines stably expressing organelle markers mt-rk and pt-rk (Nelson, Cai, & Nebenfuhr, 2007) were generated in Col-0 (#1.1 and #2.1 for mt-rk; #4.1 and #5.3 for pt-rk), *P35S:ANP1-GFP* (#2.1 and #5.1 for mt-rk; #3.2 and #7.1 for pt-rk) and *P35S:ANP3-GFP* (#8.1 and #16.1 for mt-rk; #18.1 and #28.1 for pt-rk) background.

Transient expression of px-rk organelle marker (Nelson et al., 2007) in seedlings was performed as previously described with slight modifications (Li, Park, Von Arnim, & Nebenfuhr, 2009). Cell walls were stained with propidium iodide [PI, (Naseer et al., 2012)].

2.3 | Subcellular fractionation and organelle enrichment

Ten-day-old seedlings expressing ANP1-GFP, ANP3-GFP or GFP were grown in 250 mL flasks containing 100 mL of 0.5 × MS (Murashige and Skoog, 1962) medium supplemented with 0.5% sucrose (pH 5.7) and approximately 30 mg seeds/flask. Seedlings were treated for 30 min with H$_2$O (control) or OGs (100 μg/mL). Approximately 10 g of freshly collected seedlings were homogenized by using a waring blender by adding 20 mL of freshly prepared extraction buffer (pH 7.8) containing; 30 mM MOPS 0.3 M mannitol, 1 mM EDTA, 0.2% BSA, 0.6% PVP, 4 mM Cysteine, 1 mM phenylmethylsulphonyl fluoride (PMSF), 1× Protease inhibitor cocktail (Sigma Aldrich P9599), and 1× Phosphatase inhibitor cocktail (Sigma Aldrich P2850). The homogenate was filtered twice by using 40 μm nylon mesh and the flow through collected in a cold 50 mL screw cap tube.

Nuclei were collected after a first centrifugation (5 min, 100 × g at 4°C) as a grey pellet that was re-suspended by using a paintbrush and processed as described below. The supernatant obtained from the first centrifugation was used to obtain chloroplasts and centrifuged 15 min at 3000 × g at 4°C. A green pellet was carefully resuspended in 5 mL of cold extraction buffer by using a small paintbrush. The chloroplast suspension was gently loaded on a new 50-ml screw cap tube containing a discontinuous Percoll gradient [top to bottom: 10% (2 mL), 40% (2.5 mL) and 80% (2.5 mL)] and rapidly subjected to a fixed angle centrifugation (15 min, 10000 × g at 4°C). Damaged and broken chloroplasts at the 10–40% interface were

discarded, while intact chloroplasts formed a greenish band at the 40–80% interface that was collected and transferred in a new 15 mL screw cap tube. Chloroplasts were washed twice to remove the Percoll solution by adding 3 volumes of extraction buffer and centrifuging for 7 min at $10000 \times g$ at $4°C$ and finally resuspended in 200 μL of extraction buffer. The nuclear suspension was loaded on a 2 mL glass microcentrifuge tube containing a discontinuous Percoll gradient [top to bottom: 40% (600 μL) and 80% (600 μL)] and subjected to ultracentrifugation in a TLS-55 Rotor, Swinging Bucket (15 min, $14000 \times$ rpm at $4°C$). Nuclei collected at the 40%/80% Percoll interphase were resuspended twice in 2 mL extraction buffer, centrifuged for 2 min at $1000 \times g$ in a fixed angle rotor ($4°C$) and finally resuspended in 200 μL of extraction buffer. Preparation of mitochondria was performed in the extraction buffer described above, from 10 g of 10-day-old flask-grown seedlings. Seedlings were homogenized in 25 mL extraction buffer and subjected to 3 different centrifugations (a); 5 min, $100 \times g$; b) 10 min, $3,000 \times g$; 15 min, $10000 \times g$ at $4°C$. The supernatant was divided into 2-ml cap tubes and subjected to a last centrifugation in a fixed angle centrifuge (20 min, $20,000 \times g$ at $4°C$). Pellets were resuspended in the extraction buffer, pooled in a 2 mL glass microcentrifuge tube containing a discontinuous Percoll gradient [top to bottom: 20% (600 μL) and 30% (600 μL) Percoll supplemented with 0.25 M sucrose] and subjected to ultracentrifugation in a TLS-55 Rotor, Swinging Bucket (20 min, 40,000 rpm at $4°C$). Mitochondria were collected at the interphase 40%/80% Percoll interphase. The suspension was brought to 2 mL with extraction buffer and centrifuged for 2 min at $20000 \times g$ in a fixed angle rotor ($4°C$).

Following organelle enrichment, 1 mM DTT and SDS were added to a final concentration of 4%. Samples were briefly vortexed and kept in ice for 10 min before protein quantification.

2.4 | Western blot analyses

Upon organelle separation and protein solubilization, proteins were quantified by Bradford Assay (Biorad). The sample volume corresponding to the indicated protein amounts was boiled for 5 min after the addition of the Laemmli buffer, briefly vortexed and centrifuged (30 sec at maximum speed) before loading onto the gel. Proteins were resolved on 12% polyacrylamide gels, transferred onto a nitrocellulose membrane (semi-dry Trans-Blot Turbo-Biorad), which was then blocked by incubation with 5% BSA in 1× TBS-T for 1 h. The presence of GFP was determined using primary specific antibodies (α-GFP Agrisera AS15 3,001). Specific organelle markers were detected by using antibodies against TIC40 (α-TIC40, Agrisera AS010 709) for chloroplasts, histone H3 (α-histone H3, Agrisera AS10 710A) for nuclei, AOX1/2 (α-AOX1/2, Agrisera AS04 054) for mitochondria and cFBPase (α–cFBPase, Agrisera AS04 043) for the cytosol. All the antibodies were dissolved in BSA-1%-TBS-T buffer. With the exception of α-GFP (HRP conjugated), α-rabbit-HRP (Amersham ECL) in TBS-T was used to detect α-TIC40, α-H3 and α-AOX1/2 corresponding signals. The concentrations of the antibodies as well as

the timing of incubation were selected accordingly to the manufacturer protocols.

For total ANP protein detection upon OG (100 μg/mL) treatments, 10-day-old seedlings were grown in 250 mL Erlenmeyer flasks containing 100 mL 0.5 x MS medium supplemented with 0.5% sucrose (pH 5.7). The expression analysis and protein extraction of ANP1-GFP, ANP3-GFP or cytosolic GFP-expressing seedlings was performed as follows: seedlings were either immediately flash frozen in liquid nitrogen or frozen after 60 min treatment with H_2O (control), 30 min OG (100 μg/mL), or a combination of 30 min treatment with 10 μM Cycloheximide (CHX; Sigma-Aldrich C4859, dissolved in DMSO and further diluted in MS/2 to generate an aqueous CHX working solution) followed by 30 min OG application. Upon treatments, seedlings were ground with a MM301 Ball Mill (Retsch). ANP1/ANP3-GFP fusion proteins were extracted by using a modification of the extraction buffer described by Yamasaki, Shimoji, Ohshiro, and Sakihama (2001). The buffer contained 10 mM KH_2PO_4, 0.3 M mannitol, 25 mM sodium pyrophosphate, 1 mM EDTA, 0.2% BSA, 0.5% PVP, 4 mM cysteine, 1 mM phenylmethylsulphonyl fluoride (PMSF), 1× Protease inhibitor cocktail (Sigma Aldrich P9599) 1× Phosphatase inhibitor cocktail (Sigma Aldrich P2850), [(pH 7.6)] supplemented with 2.5 mM DTT. Protein extracts were centrifuged (30 min, $13,000 \times g$ at $4°C$) in a fixed angle centrifuge (Allegra 64R-Beckman Coulter). Proteins were quantified by using the Bradford Assay (Biorad). After quantification, 2X Laemmli buffer was added to the samples and proteins were resolved in 10% SDS-Page gels and transferred onto a nitrocellulose membrane. The presence of GFP was determined as described above. Pretreatment with the proteasome inhibitor MG132 (100 μM - Sigma-Aldrich, M7449 in DMSO) was performed overnight on 9-day old flask-grown seedlings. Equivalent volumes of nylon-filtered DMSO were supplemented to flasks containing control seedlings (mock treatments). OG treatment (100 μg/mL, 30 min) was performed the day after. Protein extraction, quantification and western blots were performed following the same steps described before. In order to evaluate equal loading, monoclonal α-actin antibody was used (Sigma Aldrich A0480).

2.5 | Gene expression analysis

Gene expression analyses were performed as previously described (Savatin et al., 2014a) with slight modifications. Seedlings or leaf tissues were frozen in liquid nitrogen and homogenized with a MM301 Ball Mill (Retsch). Total RNA was extracted from at least 3 independent biological replicates, each composed of 20 seedlings or at least 3 adult leaves from different plants, with Isol-RNA Lysis Reagent (5 Prime) according to the manufacturer's protocol. Total RNA (2 μg) was treated with RQ1 DNase (Promega) and first-strand cDNA was synthesized using ImProm-II reverse transcriptase (Promega) according to the manufacturer's instructions. Quantitative RT-PCR analyses were performed by using a CFX96 Real-Time System (Bio-Rad). cDNA (corresponding to 50 ng of total RNA) was amplified in a 30 μL reaction mix containing 1× GoTaq Real-Time PCR System

(Promega) and 0.4 μM of each primer. Three technical replicates were performed for each sample and data analysis was done using LinRegPCR software. Expression levels of each gene, relative to *UBQ5*, were determined using a modification of the Pfaffl method (Pfaffl, 2001) as previously described (Ferrari, Galletti, Vairo, Cervone, & De Lorenzo, 2006) and expressed in arbitrary units.

2.6 | Confocal laser scanning microscopy analyses

For confocal microscopy analyses, seedlings were grown for 6 days in Petri dishes containing 0.5x MS supplemented with 1% sucrose and 1% plant agar. To induce the silencing of ANP1 in amiR1 plants 1 μM of β-estradiol was added to the medium. DMSO (0.1% v/V) alone was used as control.

Treatments with elicitors were performed by immersing the entire seedling in 500 μL of water (control) or water containing OGs (100 μg/mL) or elf18 (100 nM) for the indicated times. Cotyledons were then detached and mounted on a slide in the solution in which they were last treated. Staining with propidium iodide (PI; Life Technologies) was performed by adding the dye (2 μg/mL, final concentration) to the elicitor solution and incubating cotyledons for 10–15 min before mounting. For ROS detection, cotyledons were immerged in 2′,7′-dichlorofluorescein-diacetate (DCF-DA, BioChemika; 100 nM in water) for 2 min after elicitor treatment and before mounting. All stock solutions were kept at −20°C and working solutions were prepared fresh before use.

Confocal analyses were performed using an inverted laser scanning confocal microscope (LSM780 NLO; Carl Zeiss or SP8X; Leica). Imaging of ANP-GFP, mt-rk (ABRC-Arabidopsis Biological Resource Centre), pt-rk (ABRC), DCF-DA and PI were performed using 488-nm excitation of an Argon ion laser (25 mW) for GFP and 543-nm He/Ne laser (5 mW) for mCherry, NLS-RFP and PI; a 488/543/633 beam splitter was used for acquisition. Imaging was performed using the objective 40× Zeiss plan-neofluar oil, 1.3 NA, DIC or HC PL APO CS2 40×/1.10 Water-Corrected Objective-Leica. Autofluorescence was detected in far red upon excitation with 488-nm of an Argon ion laser. All images are representative of at least five independent experiments.

Mean fluorescence intensity of cotyledons expressing ANP-GFP and those expressing the soluble GFP was obtained by merging 30 optical sections (0.3 μm step interval) of a Z-stack acquired by the LSM780 NLO confocal microscope at the same laser gain setting. Background fluorescence (mainly due to the chloroplast and stomata) was determined in wild type seedlings and subtracted from the fluorescence mean intensity measured in the transgenic plants.

2.7 | Bioinformatic analyses

Localization prediction were performed by using PSORT (http://psort.hgc.jp/form.html) and Mitoprot (http://ihg.gsf.de/ihg/mitoprot.html) The ambiguous targeting predictor (ATP - http://www.plantco.de/

gtp/) was also used, which considers 12 different amino acid properties previously described to significantly contribute to the dual targeted protein localization, for example, alpha helix, random coil, negative residues and arginine (Mitschke et al., 2009). Three on-line bioinformatics "integrators" programs [WolfPsort (https://wolfpsort.hgc.jp/), ProtComp Version 9.0 (http://www.softberry.com/berry.phtml?topic=protcomppl&group=help&subgroup=proloc) and Cello v2.5 (http://cello.life.nctu.edu.tw/)], reported to correctly predict peroxisomal localization even in the absence of canonical peroxisomal targeting signal (Chen, Teng, & Xiao, 2017) were also used. Putative protein ubiquitination sites were searched using UbPred (Radivojac et al., 2010),

2.8 | Accession numbers

Sequence data from this article can be found in the Arabidopsis Genome Initiative under accession numbers: AT3G62250 (*UBQ5*), AT1G09000 (*ANP1*), AT1G54960 (*ANP2*), AT3G06030 (*ANP3*).

3 | RESULTS

3.1 | ANP3 localizes in mitochondria and both ANP1 and ANP3 localize in plastids and nucleus upon elicitation

In order to gain insight into the function of ANPs, we stably expressed GFP-tagged forms of ANPs in wild-type Arabidopsis plants and the expression of the GFP alone was used as a control. Because fluorescence was not detectable by laser scanning confocal microscopy (LSCM) in T1 plants transformed with constructs that carried the native promoters to drive ANP-GFP expression, the protein fusions were placed under the control of the *CaMV 35S* promoter. No fluorescence signal could be detected in the case of ANP2-GFP, under either its native promoter or the *CaMV 35S* promoter, in the transgenic plants. Two homozygous T3 lines carrying a single insertion and showing fluorescence (lines #38.1 and #24.1 for *P35S:ANP1-GFP*; #4.9 and #8.1 for *P35S:ANP3-GFP*; #1.1 and #2.1 for the control construct *P35S:GFP*) were selected. These plants are hereon indicated simply as ANP-GFP and GFP plants. The presence of transgene transcripts was also assessed by quantitative RT-PCR (qRT-PCR) analysis and by using *GFP*–specific primers (Figure S1A).

The subcellular localization of the GFP-tagged ANP1 and ANP3 in epidermal cotyledon cells of the transgenic plants was assessed by LSCM analysis. In normal conditions, seedlings expressing ANP1-GFP showed a diffuse fluorescence in the cytosol and a faint fluorescence in a large structure likely corresponding to the nucleus (Figure S2A; movie S1). Seedlings expressing ANP3-GFP showed a punctate fluorescence mainly restricted to small motile bodies that were distributed in the cortical cytoplasm (Figure S2A, arrows; movie S2), leaning to the plasma membrane likely due to the presence of the large central vacuole. The signal was faint and mostly associated with chlorophyll

fluorescence in wild type, non transformed, Columbia-0 control seedlings [Figure S2A; (Tejos, Mercado, & Meisel, 2010)], whereas was intense and distributed throughout the cytosol and in the nucleus in GFP-expressing seedlings (Figure S2A), in agreement with literature data (Hanson and Kohler, 2001).

Elicitation with OGs or elf18 led to a change in the localization of ANP1 and ANP3 fluorescence, which appeared for both proteins in discoid bodies that were mobile and often organized in pairs (Figure S2B, empty arrows). ANP3 fluorescence also appeared in the large structures, presumably nuclei, and generally located in the mid to the lower sections of each cell (Figure S2B, stars). In both fluorescent ANP fusions, some of the labelled discoid bodies were stably associated with the putative nuclei (Figure S2B and C, see empty arrows; movie S3 and S4 for OGs and S5 and S6 for elf18). ANP3 fluorescence associated with the small motile bodies visible in optical section at the level of the cortical cytoplasm remained similar to that observed in non-elicited conditions, whereas ANP1 fluorescence was never observed in a similar location. Treatments with oligomannuronides and tri-galacturonic acid, known to be elicitor-inactive wall-derived molecules, did not lead to changes in the localization of fluorescent ANP1 and ANP3 (Figure S2D). Both independent lines for each construct showed a similar behavior upon treatment with the elicitors. Elicitation did not affect either the fluorescence in the GFP-expressing control line or in Col-0 (Figure S2E).

The nature of the labelled bodies and organelles was determined by co-localization experiments in stable transformed ANP-GFP transgenic seedlings with a nuclear marker [red fluorescent protein fused to a nuclear localization signal (NLS-RFP)], a mitochondrial (mt-rk) and a plastidial marker (pt-rk), both fused to mCherry (Nelson et al., 2007) (Figure 1; movie S1). The largest labeled structures identified in ANP1-GFP seedlings in both basal and elicited conditions (Figure 1a, b) as well as in ANP3-GFP (Figure 1b) upon elicitation were confirmed to be nuclei, due to ANP colocalization with NLS-RFP. The small motile bodies with which ANP3, but not ANP1, was found to be associated in both non-elicited and elicited cells showed co-localization with mt-rk and were therefore identified as mitochondria (Figure 1a, b). The discoid organelles observed in elicited cells expressing ANP1-GFP and ANP3-GFP were labeled by pt-rk, and therefore corresponded to plastids that are typical of epidermal cells (Figure 1b). ANP1 and ANP3 fluorescence was not observed in plastid stromule-like structures, suggesting that ANPs are not localized in the stroma in these organelles. Moreover, no co-localization of ANP3-GFP was observed with a peroxisomal marker (px-rk) (Nelson et al., 2007) (Figure S3A and movie S7).

Whether the observed relocalization of the fluorescent proteins requires de novo protein synthesis was assessed by LSCM analysis, after a pre-treatment of the cotyledons with cycloheximide (CHX), a well-known inhibitor of protein biosynthesis (Schneider-Poetsch et al., 2010) before elicitation with OGs. The effectiveness of CHX was first tested by monitoring the decrease of the fluorescence mean intensity in non-elicited ANP-GFP seedlings in a time course analysis. Fluorescence decreased by about 20% already after 30 min for both fusion proteins and by about 38% and 45% at 60 min for ANP1-GFP and ANP3-GFP, respectively (Figure S3B). Seedlings were then treated with CHX followed by incubation with OGs, elf18 or H_2O (control). Relocalization of ANP3-GFP to plastids and nuclei as well as the mutual association of these organelles was not significantly affected by the presence of the inhibitor (Figure S3C), suggesting that changes in the localization of ANPs do not involve newly synthesized protein.

In order to corroborate the evidence that ANPs relocalize upon elicitation, we next investigated the localization dynamics of ANP proteins by subcellular fractionation experiments followed by western blot (WB) detection, using an anti-GFP antibody. Seedlings of the ANP lines showing the higher transcript levels (ANP1-GFP #38.1 and ANP3-GFP #4.9) were used in these analyses. A suitable extraction buffer was defined for the extraction of intact fluorescent ANP1 and ANP3; this allowed the detection of bands corresponding to the expected size by SDS-PAGE and WB analyses, with no visible degradation of the fusion proteins. Next, we isolated nuclei, chloroplasts and mitochondria from ANP1-GFP or ANP3-GFP seedlings treated with OGs or H_2O for 30 min, and proteins were extracted and analyzed by WB analyses using the anti-GFP antibody as well as antibodies against organelle-specific marker proteins. Both ANP1 and ANP3 were detected in protein fractions enriched in nuclei or chloroplasts only after OG treatment (Figure 2a). Moreover, ANP3 was found in the mitochondrial fraction, independently of the presence of the elicitor, whereas ANP1 was not found in these organelles (Figure 2b). These results are consistent with the intracellular localization data obtained by LSCM.

3.2 | The fluorescent ANP fusions are functional, expressed at very low levels and regulated at the post-translational level

The functionality of the tagged proteins was verified by analyzing the capability of the *P35S:ANP1-GFP* and *P35S:ANP3-GFP* constructs to complement the defective defense responses of the *anp1 anp2* and *anp2 anp3* double mutants (Savatin, Gigli-Bisceglia, et al., 2014a). Basal susceptibility to *B. cinerea* and elicitor-induced responses, such as protection against this fungus and ROS production, were restored to wild-type levels upon the expression of ANP1-GFP and ANP3-GFP in both types of double mutant plants (Figure S4a,b). Moreover, the expression of ANP3-GFP but not of GFP alone rescued the cytokinesis-related defect (cell wall stubs) and the reduced root length that are typical of the *anp2 anp3* mutant (Figure S4c,d).

Even though the expression of the ANP-tagged proteins was driven by the *CaMV 35S* promoter, all the analyses we have performed showed very low expression level of the tagged protein in the transgenic plants, thus making unlikely the possibility that the observed effects were artifactual and due to ANPs overexpression. Analyses of ANP-GFP cotyledons confirmed that the fluorescence level was considerably lower when compared to that of control GFP ones (Figure S1b). Similarly, WB analyses of the expression levels of the tagged proteins in the transgenic plants showed that the intensity
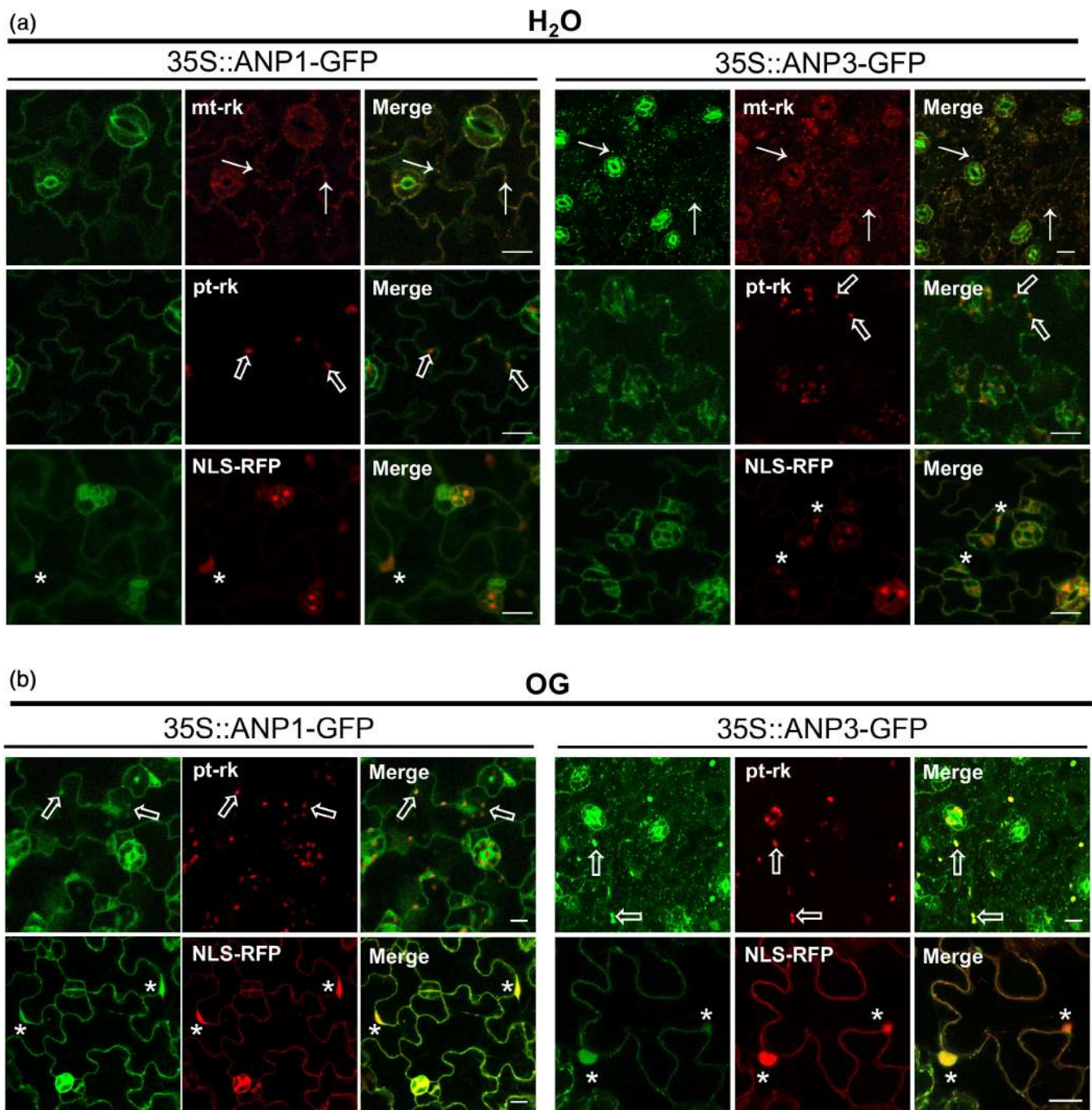
FIGURE 1 ANP3, but not ANP1, is localized in mitochondria in non-elicited conditions and both proteins display a similar subcellular relocalization to plastids and nuclei upon elicitation. Five-day-old cotyledons stably co-expressing ANP1-GFP or ANP3-GFP and different red-fluorescent organelle markers [mitochondria (mt-rk), plastids (pt-rk) or nuclei NLS-RFP] were analyzed by LSCM. (a) In non-elicited conditions, ANP1-GFP shows diffuse fluorescence in the cytoplasm and a faint fluorescence in the nucleus (stars) and no co-localization with mitochondria (white arrows) or plastids (empty arrows). On the other hand, ANP3 plants display punctate fluorescence restricted in small bodies, which show co-localization (merge) only with mt-rk. (b) Upon treatment with OG, both ANP-GFP proteins are visible in discoid bodies (empty arrows) often associated to large spherical structures (stars). Co-localization analyses show that both ANP-GFP fusions co-localize with the red fluorescent organelle marker pt-rk (empty arrows in upper panels) and with the NLS-RFP marker (stars in bottom panels). A similar localization was observed after treatment with elf18. Bar = 20 μm (a) and 10 μm (b)

of the ANP-GFP bands was at least 100-fold lower that the GFP band of the control plant extracts (Figure 3a), indicative of a very low steady-state level of the ANP fusions.

The analysis of total fluorescence also showed an increase in both ANP1 and ANP3 signals upon elicitation with OGs or elf18 (Figure 3b), Indeed, in WB analyses, the intensity of both ANP1-GFP
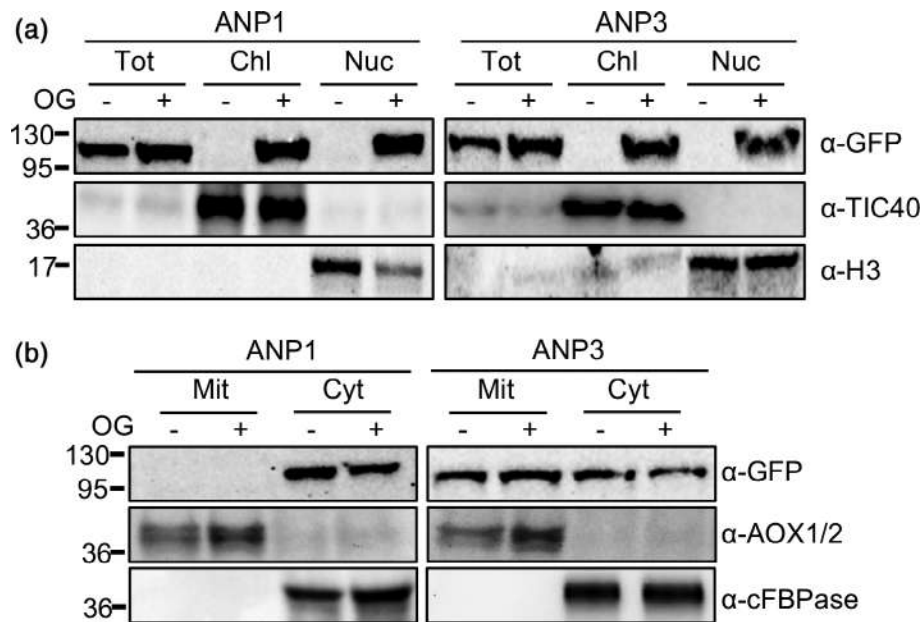
FIGURE 2 Subcellular fractionation and immunoblot analyses show relocalization of ANP1 and ANP3 upon OG treatment. Seedlings expressing either ANP1-GFP or ANP3-GFP were treated (+) for 1 hr with OGs before organelle preparation. Western blot analysis was performed using a GFP-specific antibody (α-GFP). (a) Total proteins (Tot; 200 μg), chloroplast proteins (Chl; 50 μg), and nuclear proteins (Nuc; 50 μg). (b) Proteins from a mitochondria-enriched fraction (Mit; 50 μg) and from the supernatant obtained after the centrifugation at 20.000 × g (cytosolic fraction, Cyt; 200 μg). The same protein amounts were analyzed in parallel by probing with (a) antibodies against the chloroplast inner envelope membrane import complex (α-TIC40) or histone H3 (α-H3) and, (b) antibodies against the mitochondrial alternative oxidase 1/2 (α-AOX) and fructose-1,6-bisphosphatase as a cytosolic marker (α–cFBPase)

and ANP3-GFP protein bands increased upon treatment with OGs for 30 min (Figure 2c). The increase also occurred when the OG treatment was performed after pre-incubation with CHX (Figure 3c), suggesting that, rather than on *de novo* synthesis, the OG-induced increase of ANP proteins might depend on a reduced degradation possibly mediated by the proteasome, a behaviour previously described for MEKK1 (Nakagami et al., 2006). However, the increase of the ANP1-GFP and ANP3-GFP band intensity in response to OGs occurred also in the presence of the proteasome inhibitor MG132. Notably, ANP levels increased upon MG132-treatment in both non-elicited and elicited conditions (Figure 3d). Thus, proteasome-dependent degradation appears to regulate ANP levels, even if this mechanism is unlikely to be responsible for the elicitor-induced increase of the protein amounts.

3.3 | Organelle targeting of ANP1 and ANP3 is directed by the N-terminal sequence

The observed localization of ANP1 in cytosol, nuclei and plastids, and of ANP3 in the same organelles as well as in mitochondria is consistent with predictions provided by the SUBcellular localization database for Arabidopsis proteins (SUBA3 - http://suba.plantenergy.uwa.edu.au/), and with a proteomic study reporting the presence of ANP3 in plastids (Ferro et al., 2010). On the other hand, the observed lack of localization in peroxisome is in agreement with bioinformatics analyses performed using three on-line bioinformatics "integrators" programs [WolfPsort, ProtComp Version 9.0. and Cello v2.5], widely used to predict targeting signal and subcellular localization and capable of correctly predicting peroxisomal localization even in the absence of a canonical peroxisomal targeting signal (Chen et al., 2017). None of them provided any indication of peroxisomal localization.

In most cases, a region of about 60–80 amino acids at the N-terminus targets proteins to mitochondria and plastids (Kim & Hwang, 2013). However, different software for protein subcellular localization prediction failed to find, in both ANP1 and ANP3 amino acid sequences, specific patterns that might be required for ANP protein sorting to mitochondria or plastids. This is not unexpected because predictors can identify only a small fraction of localization sequences (Mitschke et al., 2009; Nguyen Ba, Pogoutse, Provart, & Moses, 2009), and because ANP1 and ANP3, which display a multiple localization, may contain ambiguous localization sequences, which are often undetectable by predictors (Berglund, Pujol, Duchene, & Glaser, 2009; Carrie & Small, 2013). Analysis with Ambiguous Targeting Predictor (ATP), which produces scores >0.7 for univocally targeted proteins and > 0.3 for proteins that are ambiguously targeted (Mitschke et al., 2009), produced a score of 0.49 for ANP1 and 0.57 for ANP3. Localization to mitochondria is predicted with a higher confidence for ANP3 compared to ANP1 also by both PSORT (0.657 and 0.431, respectively) and Mitoprot (0.660 and 0.416, respectively) (Claros & Vincens, 1996).

We therefore experimentally addressed whether the N-terminus sequence of both ANP1, and ANP3 is responsible for their observed
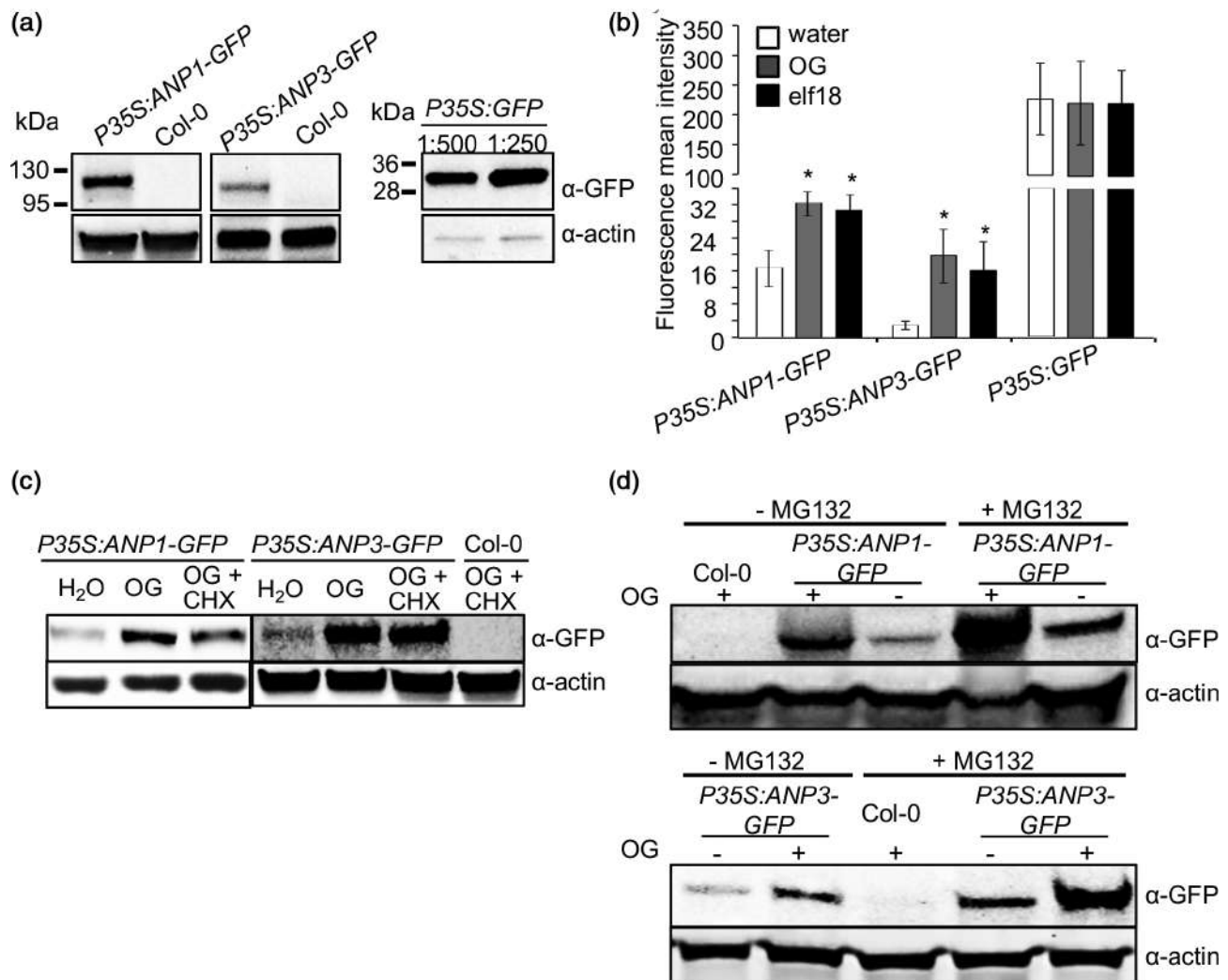
FIGURE 3 ANP1 and ANP3 are expressed at low level and subject to post-translational regulation. (a) ANP1 and ANP3 are expressed at low level compared to the GFP (control). Western blot analysis of total proteins from seedlings expressing ANP-GFP or GFP. To obtain bands of comparable intensity, extracts from seedlings were diluted 1:250 and 1:500. (b) Elicitor-triggered accumulation of ANPs is confirmed by the fluorescence mean intensity measured by LSCM in cotyledons of 5-day-old ANP-GFP and GFP seedlings. Average of three independent experiments (n = 12 cotyledons) is presented in the graph. Asterisks indicate statistically significant differences between treated and untreated samples, according to Student's *t* test (*p < .05). (c) ANPs accumulate in response to OG. Western blot analysis of total protein extracts from seedlings treated for 60 min with H2O or OGs in the presence or in the absence of cycloheximide (CHX), which was added 30 min before treatment with the elicitor. (d) ANP1 and ANP3 are regulated by proteasome-mediated degradation both in the presence and in the absence of OGs. Col-0, ANP1-GFP, and ANP3-GFP seedlings were treated for 1 hr with OGs in the presence or in the absence of the proteasome inhibitor MG132. Total protein extracts were analyzed by Western blot. In all Western blot analyses, ten-day-old seedlings were used. ANP-GFP fusions were detected using an antibody against GFP. Actin levels were determined to evaluate the equal loading

localization in these organelles. Co-localization analyses were performed in transgenic Arabidopsis plants co-expressing mt-rk or pt-rk marker and a GFP fusion with the first 68 aa of ANP1 (ANP1NT68-GFP) or the 67 of ANP3 (ANP3NT67-GFP) both representing the region that precedes the conserved serine/threonine kinase catalytic domain (Figure 4a). Results showed that ANP1NT68-GFP localized to cytosol and plastids, whereas ANP3NT67-GFP localized to mitochondria, cytosol, and plastids (Figure 4b and movie S8 and S9).

On the other hand, the truncated (Δ) ANP1 and ANP3 version lacking the N-terminal region (ΔNT68ANP1-GFP and ΔNT67ANP3-GFP)

showed cytosolic and nuclear localization only (Figure S5 and movies S10, S11). These analyses indicate that the N-terminal region is capable of directing ANPs to mitochondria and plastids.

3.4 | Elicitor-induced accumulation of ROS in mitochondria, plastids and nuclei is abolished in ANP triple mutants

ANPs have been shown to mediate response to hydrogen peroxide (Kovtun et al., 2000; Savatin, Gigli-Bisceglia, et al., 2014a) and to be
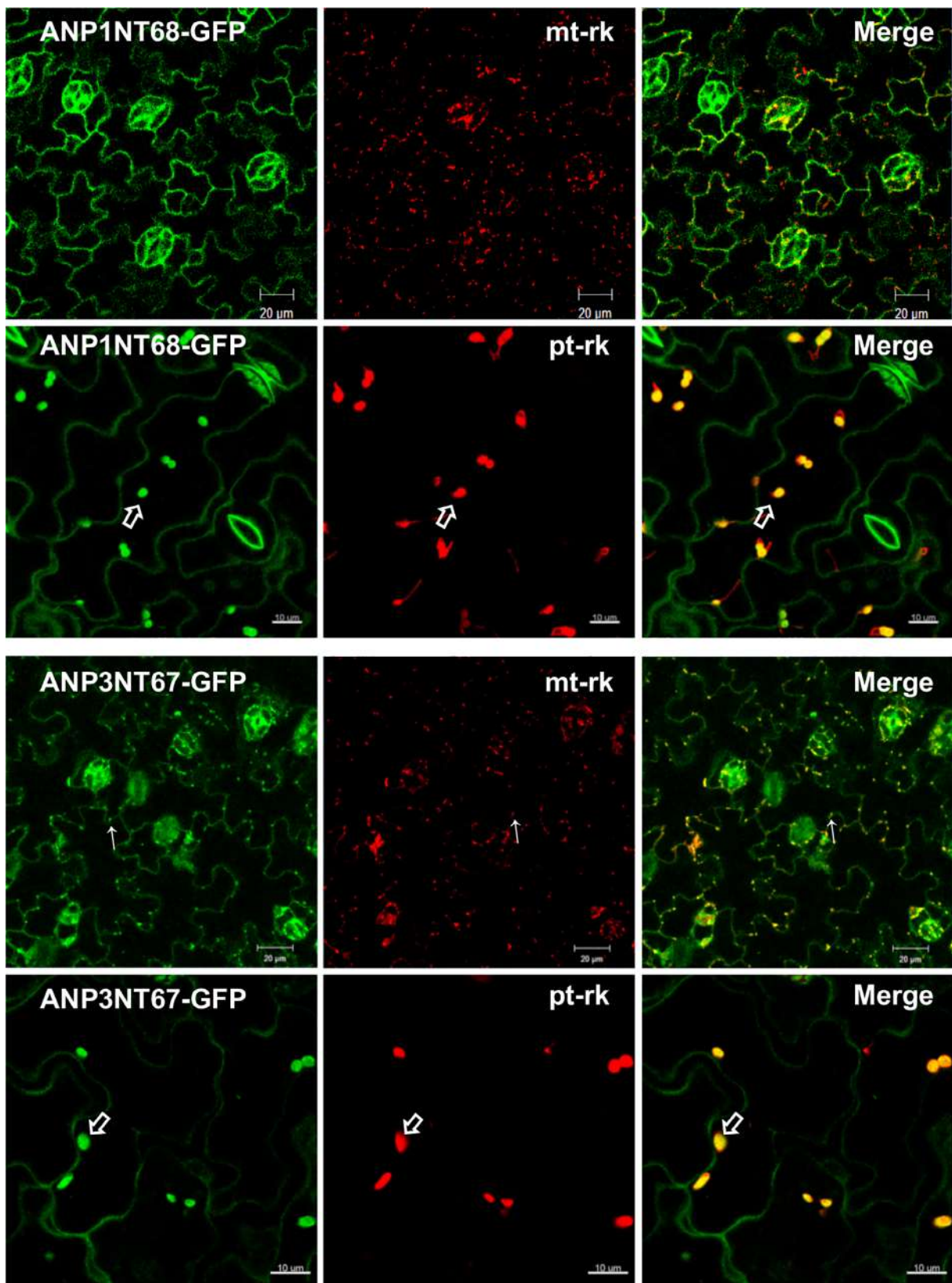
FIGURE 4 The N-terminal region is sufficient for localization of ANP1 to plastids and of ANP3 to both mitochondria and plastids. (a) The 68- and 67-amino acid N-terminal sequence of ANP1 and ANP3, respectively, excluding the conserved kinase region. (b) Co-localization analyses by LSCM in cotyledon epidermal cells of transgenic seedlings stably co-expressing protein fusions between the ANP N-terminal portions shown in (a) and GFP (*P35S:ANP1NT68-GFP*; *P35S:ANP3NT67-GFP*) and the mitochondrial (mt-rk) or plastid (pt-rk) marker. See also movies S8 and S9

redundantly required for elicitor-induced production of extracellular ROS (Savatin, Gigli-Bisceglia, et al., 2014a). Because plastids and mitochondria as well as nuclei are known sites of ROS generation (Mazars, Thuleau, Lamotte, & Bourque, 2010; Petrov & Van Breusegem, 2012; Shapiguzov, Vainonen, Wrzaczek, & Kangasjarvi, 2012), we investigated whether the association of ANP1 and ANP3 reflects a role in the regulation of ROS generated or accumulated in these organelles, by using the previously generated conditional *anp* triple mutant amiR1 (Savatin, Gigli-Bisceglia, et al., 2014a).

Accumulation of intracellular ROS in response to OGs was first analyzed by LSCM in wild-type cotyledons expressing mt-rk or pt-rk and stained with 2-7-dichlorofluorescein diacetate (DCF-DA). Upon elicitation, fluorescence appeared in small motile bodies corresponding to mitochondria, mostly visible in cortical optical sections (Figure S6a), as well as in plastids (Figure S6b) and nuclei (Figure S6c), both detectable in deeper cell sections. The OG-induced fluorescence pattern was very similar to that induced by elf18 (Figure 5) and strikingly similar to that observed in OG- and elf18-treated cells expressing fluorescent ANP3 (see Figure 1b). No detectable fluorescence was observed in these organelles in non-elicited cotyledons (Figure S6a,b upper panel; water control).

Next, the presence of ROS was analyzed in mutant seedlings grown in the presence of β-estradiol, treated with OGs, elf18 or water and then stained with DCF-DA. Wild-type seedlings showed fluorescence in mitochondria, plastids and nuclei (Figure 5) only upon treatment with OGs or elf18. On the contrary, no fluorescence appeared in mitochondria, plastids and nuclei in elicited amiR1 triple mutant seedlings (Figure 5). Taken together, these data indicate that ANPs are required not only for the extracellular but also for the intracellular ROS accumulation triggered by OGs and elf18.

4 | DISCUSSION

This work deepens our understanding of the biology of ANPs by providing knowledge about their subcellular localization and dynamics in physiological conditions and upon elicitation. Although MAP kinase cascades represent highly conserved signaling modules in all
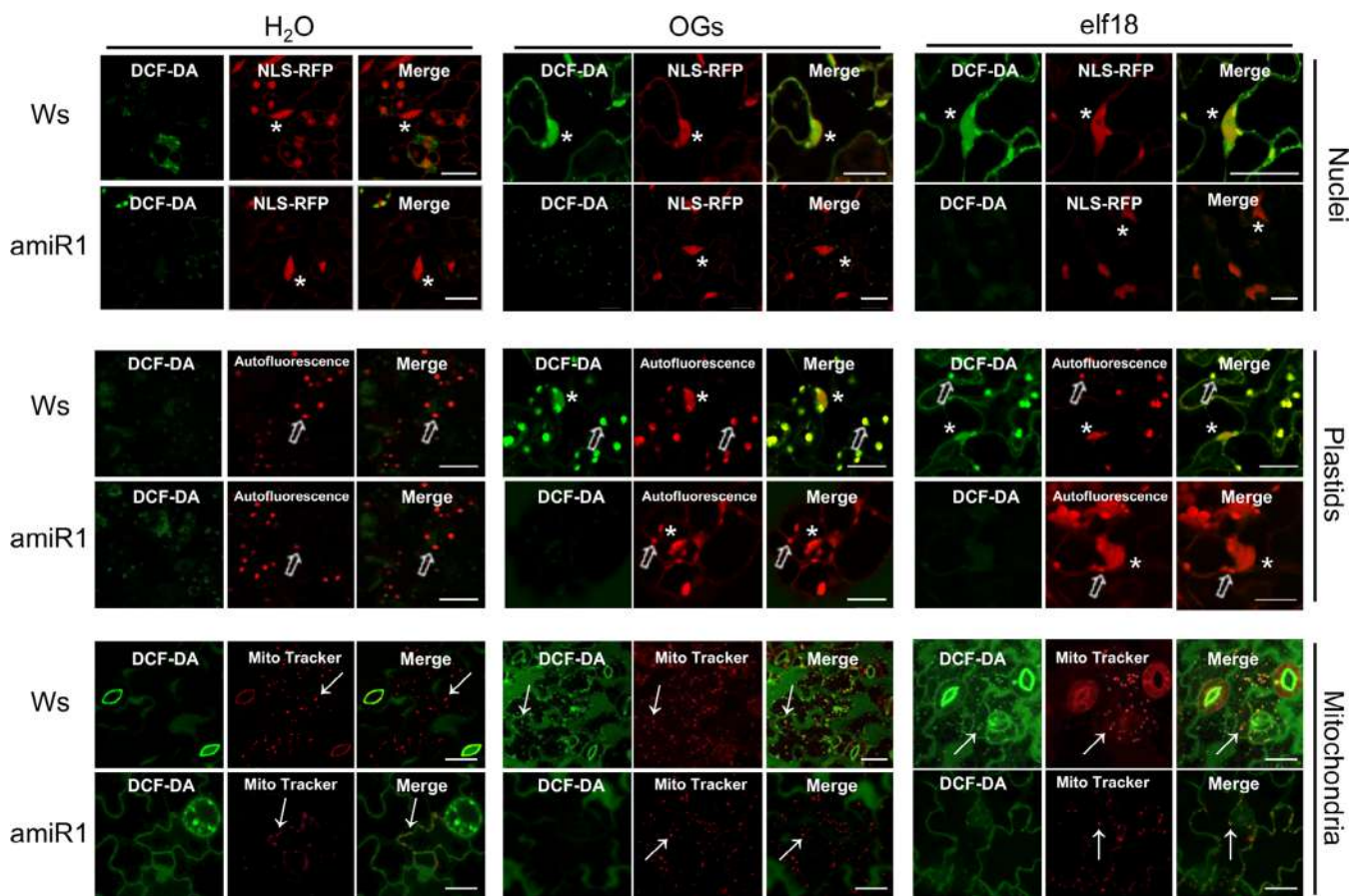

FIGURE 5 Silencing of the *ANP* gene family leads to a reduced elicitor-triggered intracellular ROS accumulation. Silencing of *ANP1* was induced by growing amiR1 seedlings in the presence of 1 μM of b-estradiol. The wild type (Ws) was grown in a similar manner. Detached cotyledons were treated with water, OGs or elf18 and accumulation of ROS was detected by staining with the cell-permeant 2′,7′-dichlorodihydrofluorescein diacetate (DCF-DA) and LSCM analysis. Nuclei were detected by using transgenic lines stably expressing NLS-RFP marker, plastids were detected by acquiring the autofluorescence in far red whereas the Mito Tracker dye was used to detect mitochondria. Bar = 20 μm

eukaryotes, much is still unknown about the action of plant MAPKKK and more in general of MAP kinases, due to a large redundancy and pleiotropic effects that complicate their characterization (Xu & Zhang, 2015). ANPs are paradigmatic in this context, because they consist of three members that are required for cytokinesis and development (Krysan et al., 2002) as well as for responses to both PAMPs and DAMPs (Savatin, Gigli-Bisceglia, et al., 2014a). So far, only for NPK1, the tobacco homolog of ANPs, localization has been described in the phragmoplast (Beck et al., 2011). A similar localization is shown by MKK6 (Takahashi et al., 2010).

4.1 | ANPs are relocalized in response to danger signals

Our results show that, in basal non-elicited conditions, both ANP1 and ANP3 localize in the cytosol, whereas ANP3 localizes also in mitochondria. To date, a mitochondrial localization has been shown for Arabidopsis MKK7 and MKK9, both MAPKKs (Lampard et al., 2015), but not for any plant MAPKKK or MAPK (Bigeard & Hirt, 2018; Krysan & Colcombet, 2018; Samajova, Komis, & Samaj, 2013). A mitochondrial localization has also been described for human ERK1, an immune-related MAPK, in HeLa cells, upon a proliferative stimulus (Galli et al., 2009; Wainstein & Seger, 2016). In most studies, MAP kinases appear to be localized in the cytosol or in the nucleus, or both, and their substrates in plasma membrane, cytosol, nucleus and cytoskeleton (Krysan & Colcombet, 2018).

It is striking that treatment with OGs triggers the relocalization of ANP1 and ANP3 within the cell. On elicitor treatment, both proteins appear in the nucleus and plastids, as well as in the cellular compartments in which they are found under non-elicited conditions. Localization of plant MAP kinases in plastids has never been reported before. The low level of fluorescence signals in the transgenic plants make it unlikely that our observations are explainable by major artifacts due to the use of the CaMV 35S promoter. These are also ruled out by our localization studies, performed by immunoblot analyses upon subcellular fractionation, that confirm the presence of ANP3 in mitochondria and both ANP1 and ANP3 in plastids and nuclei upon elicitation.

In both animals and plants, there are examples of migration between different subcellular compartments of MAP kinases upon their activation, most probably to allow access to their substrates and initiation of specific responses. Examples are (a) the translocation to the nucleus of PcMPK3 and PcMPK6 during innate immunity in _Petroselinum crispum_ cells treated with the peptidic elicitor Pep13 (Lee, Rudd, Macioszek, & Scheel, 2004); (b) the translocation to the nucleus of AtMPK3 and AtMPK6 in Arabidopsis in response to ozone (Ahlfors et al., 2004); (c) the translocation of both stress-induced MAPKK (SIMKK) and SIMK to cytoplasmic compartments from nuclei in _Medicago sativa_ (Ovecka et al., 2014). Interestingly, the relocalization of SIMK correlated temporally with its activation in response to salt stress (Ovecka et al., 2014). Activation of MAPKs in yeasts and mammals also involves their simultaneous transport to the nucleus.

Nuclear-localized MAPKs and MAPKKs, however, do not possess NLSs and cargo proteins may be required for their translocation to the nucleus (Dahan, Wendehenne, Ranjeva, Pugin, & Bourque, 2010; Krysan & Colcombet, 2018).

ANP3 is the only protein so far simultaneously found in cytosol, mitochondria, plastids and nucleus. Although a triple localization has been described for CrIDI1, an isopentenyl diphosphate isomerase from _Catharanthus roseus_ (Guirimand et al., 2012), this is linked to protein forms originating from two alternative transcripts. By using GFP fusions, we provide experimental evidence that 67 and 68 amino acids at the N-terminal region of ANP1 and ANP3, respectively, carry the necessary information for the localization of ANP1 into plastids, and of ANP3 in mitochondria and plastids. These observations are in line with the notion that typical chloroplast targeting signals are 30–80 amino acids long (average 58 amino acids) and typical mitochondrial signals are 20–60 amino acids long (average 42 amino acids) (Kim & Hwang, 2013). In dual-targeted proteins, the N-terminal portion acts as a transit peptide (TP) essential for protein import into both organelles and generally shares features of both mitochondrial and plastid transit peptides, being often intermediate between the two (Carrie & Small, 2013). To date, a general rule for how the determinants for dual targeting are distributed within their amino acid sequence has not yet been defined (Carrie & Small, 2013; Ge, Spanning, Glaser, & Wieslander, 2014). In our western blot analyses performed on proteins extracted from isolated organelles, we did not detect significant variation in the gel mobility of ANPs, suggesting no cleavage of the N-terminal region. Several nuclear-encoded proteins imported into mitochondria and chloroplasts lack a cleavable targeting sequence (Armbruster et al., 2009; Puthiyaveetil et al., 2008; Tardif et al., 2012). However, due to the low expression levels of both ANP1 and ANP3, we cannot rule out the possibility in our conditions only a more abundant/stable fraction of these proteins is detected.

Conversely, GFP fusions of the deleted forms of ANPs lacking the first N-terminal 68/67 amino acids are localized only in nuclei and cytosol, corroborating the conclusion that the N-terminal part is responsible for organelle targeting and suggesting that sequences directing a nuclear localization are contained in the remaining part of the proteins. Indeed, predictors of eukaryotic NLSs, such as cNLS Mapper (Kosugi, Hasebe, Tomita, & Yanagawa, 2009) and NLStradamus (Nguyen Ba et al., 2009), detected putative NLS from both the ANP1 and ANP3 C-terminal sequences, but only with low cut-off scores, typical of proteins localized to both the nucleus and the cytosol (Kosugi et al., 2009). The localization in plastids and nuclei observed specifically upon elicitation suggests that the signals responsible for targeting ANPs to these compartments are not exposed before treatment or are modified in the resting state, implying different protein conformations. Indeed, the interaction between the N- and C-terminal regions of ANPs has been previously hypothesized to be responsible for an inactive state, with a conformational change being necessary for activation during cytokinesis (Komis et al., 2018; Takahashi et al., 2010).

4.2 | ANPs are regulated at the post-translational level

The treatment with OGs and elf18 not only triggers relocalization of ANP1 and ANP3, but also increases their protein levels inside the cell in a CHX- and MG132-independent manner, indicating that this is unlikely due to changes in rates of either de novo synthesis or degradation by the proteasome. Protein turnover under non-stressed conditions and stress-induced stabilization, through mechanisms not yet elucidated, have been described for the Arabidopsis MAP kinase Phosphatases 1 (MKP1) (Gonzalez Besteiro & Ulm, 2013). On the other hand, complex and multi-step regulatory mechanisms, besides ubiquitin-mediated proteolysis, control MAPKKK activity in animals (Nithianandarajah-Jones, Wilm, Goldring, Muller, & Cross, 2012).

However, we noted that levels of ANP1 and ANP3 increase upon treatment with MG132 both in the absence and in the presence of elicitors. This is consistent with the observation that high-confidence putative protein ubiquitination sites are present in their primary amino acid sequences (eleven in ANP1 and three in ANP3, localized in the C-terminal non-kinase region) and suggests a regulation at the post-transcriptional level by specific degradation. Both the low basal gene expression and the relatively short half-life (a few hours) of ANPs (see Figure S3b) compared to the predicted global protein half-life of about 4–8 days in Arabidopsis rosettes (Ishihara, Obata, Sulpice, Fernie, & Stitt, 2015; Piques et al., 2009) point to a tight regulation of their levels and function. However, the elicitor-induced increase of ANP levels does not appear to be due to ubiquitin-proteasome-dependent degradation.

4.3 | Extracellular and intracellular elicitor-induced ROS accumulation is reduced in *anp* mutants

Besides their role in cell division, ANPs are known to play a role in ROS signalling, since they are required for the response to exogenously applied H_2O_2 (Kovtun et al., 2000; Savatin, Gigli-Bisceglia, et al., 2014a) and for the elicitor-induced accumulation of extracellular ROS (Savatin, Gigli-Bisceglia, et al., 2014a). H_2O_2 and other ROS, such as singlet oxygen ($^1O_2$), superoxide $O_2^{\bullet-}$ and hydroxyl ($OH^{\bullet}$) radicals, play diverse functions in plants and animals by acting as second messengers to trigger intracellular responses, and/or as antimicrobial molecules (Sies & Jones, 2020; Waszczak, Carmody, & Kangasjarvi, 2018). Among ROS, H_2O_2 is the most stable species (half-life of more than 1 ms) and, therefore, is considered as the predominant ROS involved in cellular signaling (Mhamdi & Van Breusegem, 2018). Many studies on plant immunity have focused on extracellular ROS (Farvardin et al., 2020; Qi, Wang, Gong, & Zhou, 2017), whereas much less is known about the dynamics and the role of intracellular ROS.

ROS are produced in several plant subcellular compartments such as mitochondria, peroxisomes and chloroplasts as well as in the ER and nuclei (Wang et al., 2020; Waszczak et al., 2018). ROS accumulation in mitochondria and in chloroplasts can occur both during basal metabolism, including respiration and photosynthesis respectively, and in response to stress stimuli (Gollan, Tikkanen, & Aro, 2015; Wang et al., 2020;

Waszczak et al., 2018). Indeed, ROS generated by both mitochondria and chloroplasts have been shown to be important for plant immunity (Colombatti, Gonzalez, & Welchen, 2014; Littlejohn, Breen, Smirnoff, & Grant, 2020; Nie, Yue, Zhou, & Xing, 2015; Nomura et al., 2012) and these organelles have been proposed to act as response amplifiers upon stress stimuli (Dietz, Turkan, & Krieger-Liszkay, 2016).

The TMV-induced generation of ROS in chloroplasts of *Nicotiana tabacum* has been shown to depend on the activation of the MAP kinases SIPK/Ntf4/WIPK that culminates with HR (Liu et al., 2007). Here, we have shown that, upon elicitation, ANPs localize in the three subcellular compartments where ROS accumulate and that lack of ANPs compromises such accumulation, suggesting a functional link between ANPs and intracellular ROS homeostasis. Indeed, these kinases emerge as positive regulators of immunity-related ROS accumulation, not only in the apoplast (Savatin, Gigli-Bisceglia, et al., 2014a), but also in intracellular compartments. The involvement of ANPs in the regulation of intracellular ROS levels may at least in part account for the defects of cell division caused by their loss, since the correct organization and function of phragmoplast microtubules in cell division has been shown to require an intact ROS homeostasis (Komis, Illes, Beck, & Samaj, 2011; Livanos, Galatis, & Apostolakos, 2015; Mhamdi & Van Breusegem, 2018).

Noteworthy, analyses of the ANP fluorescence upon elicitation allowed us to detect a physical interaction between the nucleus and plastids, with several motile mitochondria located in close proximity. Similar chloroplast-nucleus interaction and clustering have been shown to occur: (a) during effector-triggered immunity (ETI) in Arabidopsis; (b) in response to flg22 and infection by RNA viruses and plant pathogenic bacteria in *Nicotiana benthamiana* (Caplan et al., 2015); (c) in response to exogenous treatment with H_2O_2 (Ding, Jimenez-Gongora, Krenz, & Lozano-Duran, 2019). The communication from organelles such as chloroplasts and mitochondria to nuclei is known as retrograde signaling (Gollan et al., 2015; Kleine & Leister, 2016; Wang et al., 2020) and is thought to integrate the activities of the different subcellular compartments (Foyer, Karpinska, & Krupinska, 2014; Mazars et al., 2010). It involves, for example, the transport of both signaling molecules, such as H_2O_2 during defense (Caplan et al., 2015; Ding et al., 2019; Exposito-Rodriguez, Laissue, Yvon-Durocher, Smirnoff, & Mullineaux, 2017), which may at least in part explain the presence of ROS in the nucleus, and regulatory proteins, such as the phosphorylated form of the transcription factor WHIRLY1 (Ren, Li, Jiang, Wu, & Miao, 2017).

Our findings open new questions about the importance of ANPs in the mitochondria-plastids-nucleus cross-talk, in the exchange of metabolites and signaling molecules between these organelles and, more in general, in the subcellular coordination of the responses to environmental stresses.

4.4 | A model for ANP subcellular dynamics

Taken together, our results may be integrated in the following model of ANP subcellular dynamics during immunity. In these proteins, the
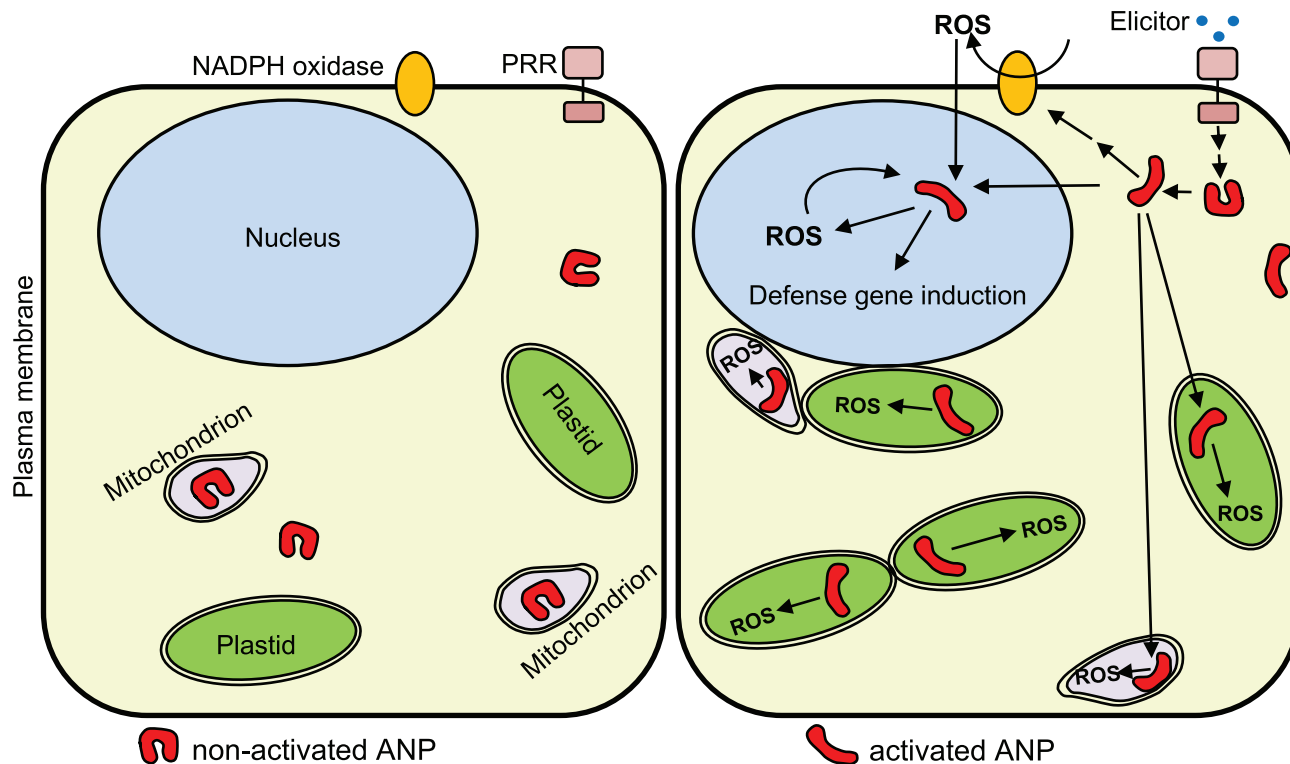
FIGURE 6 A model for ANP protein function and activation. In normal conditions (left panel), ANPs are expressed and targeted to mitochondria (ANP3 only) and cytosol (both ANP1 and ANP3), likely in a "closed", inactive conformation (resting state). Upon perception of OGs or MAMPs, ANPs undergo a conformational change from a "closed" to an "open" state (right panel) that exposes the signal sequences for translocation to plastids and nuclei. In the "open" active conformation, ANPs might regulate (directly or indirectly) NADPH-oxidase and mediate the elicitor-triggered production and response to ROS in mitochondria, plastids and nuclei

putative regulatory domain likely establishes an intra-molecular interaction with the N-terminal portion comprising the kinase domain, leading to autoinhibition and masking of the plastid and nuclear localization determinants. Upon elicitation, probably through a switching from a "closed" to an "open" conformation, the inhibition is released and the protein translocates into these organelles (Figure 6). Phosphorylation or interaction with other proteins may occur in this step, leading, for example, to a reduced affinity between domains and causing the transition of the protein to the open state. The open conformation may allow interactions with target proteins or other regulatory proteins, which, on one side, prevents ANP degradation, and, on the other, contributes to ANP relocalization.

CONFLICT OF INTEREST

Authors have no conflict of interest to declare.

AUTHOR CONTRIBUTIONS

S.D.V. and D.L.G. designed the experiments. M.L., S.D.V. and D.T.V performed microscopy analyses. M.L. and S.D.V. made the constructs and produced the transgenic lines. G.B.N. and S.D.V. performed organelle isolation, protection, gene expression and western blot analyses. D.L.G., F.C., and S.D.V. prepared the article.

ORCID

Lucia Marti https://orcid.org/0000-0003-0445-3800
Daniel-Valentin Savatin https://orcid.org/0000-0002-2165-1369
Nora Gigli-Bisceglia https://orcid.org/0000-0002-6907-1427
Valeria de Turris https://orcid.org/0000-0003-0872-185X
Felice Cervone https://orcid.org/0000-0001-8141-5352
Giulia De Lorenzo https://orcid.org/0000-0002-1707-5418

REFERENCES

Ahlfors, R., Macioszek, V., Rudd, J., Brosche, M., Schlichting, R., Scheel, D., & Kangasjarvi, J. (2004). Stress hormone-independent activation and nuclear translocation of mitogen-activated protein kinases in *Arabidopsis thaliana* during ozone exposure. *The Plant Journal*, 40, 512–522.

Armbruster, U., Hertle, A., Makarenko, E., Zuhlke, J., Pribil, M., Dietzmann, A., ... Leister, D. (2009). Chloroplast proteins without cleavable transit peptides: Rare exceptions or a major constituent of the chloroplast proteome? *Molecular Plant*, 2, 1325–1335.

Beck, M., Komis, G., Ziemann, A., Menzel, D., & Samaj, J. (2011). Mitogen-activated protein kinase 4 is involved in the regulation of mitotic and cytokinetic microtubule transitions in *Arabidopsis thaliana*. *New Phytologist*, 189, 1069–1083.

Bellincampi, D., Cervone, F., & Lionetti, V. (2014). Plant cell wall dynamics and wall-related susceptibility in plant-pathogen interactions. *Frontiers in Plant Science*, 5, 228.

Bellincampi, D., Dipierro, N., Salvi, G., Cervone, F., & De Lorenzo, G. (2000). Extracellular H2O2 Induced by Oligogalacturonides Is Not Involved in the Inhibition of the Auxin-Regulated rolB Gene Expression in Tobacco Leaf Explants. *Plant Physiology*, 122(4), 1379–1386. https://dx.doi.org/10.1104/pp.122.4.1379.

Berglund, A. K., Pujol, C., Duchene, A. M., & Glaser, E. (2009). Defining the determinants for dual targeting of amino acyl-tRNA synthetases to mitochondria and chloroplasts. *Journal of Molecular Biology*, 393, 803–814.

Bigeard, J., & Hirt, H. (2018). Nuclear signaling of plant MAPKs. *Frontiers in Plant Science*, 9, 469.

Boller, T., & He, S. Y. (2009). Innate immunity in plants: An arms race between pattern recognition receptors in plants and effectors in microbial pathogens. *Science*, 324, 742–744.

Brutus, A., Sicilia, F., Macone, A., Cervone, F., & De Lorenzo, G. (2010). A domain swap approach reveals a role of the plant wall-associated kinase 1 (WAK1) as a receptor of oligogalacturonides. *Proceedings of the National Academy of Sciences, USA*, 107, 9452–9457.

Caplan, J. L., Kumar, A. S., Park, E., Padmanabhan, M. S., Hoban, K., Modla, S., ... Dinesh-Kumar, S. P. (2015). Chloroplast stromules function during innate immunity. *Developmental Cell*, 34, 45–57.

Carrie, C., & Small, I. (2013). A reevaluation of dual-targeting of proteins to mitochondria and chloroplasts. *Biochimica et Biophysica Acta*, 1833, 253–259.

Chen, N., Teng, X. L., & Xiao, X. G. (2017). Subcellular localization of a plant catalase-phenol oxidase, AcCATPO, from Amaranthus and identification of a non-canonical peroxisome targeting signal. *Frontiers in Plant Science*, 8, 1345.

Claros, M. G., & Vincens, P. (1996). Computational method to predict mitochondrially imported proteins and their targeting sequences. *European Journal of Biochemistry*, 241, 779–786.

Clough, S. J., & Bent, A. F. (1998). Floral dip: A simplified method for agrobacterium-mediated transformation of *Arabidopsis thaliana*. *The Plant Journal*, 16, 735–743.

Colcombet, J., & Hirt, H. (2008). Arabidopsis MAPKs: A complex signalling network involved in multiple biological processes. *Biochemical Journal*, 413, 217–226.

Colombatti, F., Gonzalez, D. H., & Welchen, E. (2014). Plant mitochondria under pathogen attack: A sigh of relief or a last breath? *Mitochondrion*, 19(Pt B), 238–244.

Couto, D., & Zipfel, C. (2016). Regulation of pattern recognition receptor signalling in plants. *Nature Reviews Immunology*, 16, 537–552.

Curtis, M. D., & Grossniklaus, U. (2003). A Gateway Cloning Vector Set for High-Throughput Functional Analysis of Genes in Planta. *Plant Physiology*, 133(2), 462–469. https://dx.doi.org/10.1104/pp.103.027979.

Dahan, J., Wendehenne, D., Ranjeva, R., Pugin, A., & Bourque, S. (2010). Nuclear protein kinases: Still enigmatic components in plant cell signalling. *New Phytologist*, 185, 355–368.

De Lorenzo, G., Ferrari, S., Cervone, F., & Okun, E. (2018). Extracellular DAMPs in plants and mammals: Immunity, tissue damage and repair. *Trends in Immunology*, 39, 937–950.

Dietz, K. J., Turkan, I., & Krieger-Liszkay, A. (2016). Redox- and reactive oxygen species-dependent signaling into and out of the photo-synthesizing chloroplast. *Plant Physiology*, 171, 1541–1550.

Ding, X., Jimenez-Gongora, T., Krenz, B., & Lozano-Duran, R. (2019). Chloroplast clustering around the nucleus is a general response to pathogen perception in Nicotiana benthamiana. *Molecular Plant Pathology*, 20, 1298–1306.

Exposito-Rodriguez, M., Laissue, P. P., Yvon-Durocher, G., Smirnoff, N., & Mullineaux, P. M. (2017). Photosynthesis-dependent H2O2 transfer from chloroplasts to nuclei provides a high-light signalling mechanism. *Nature Communications*, 8, 49.

Farvardin, A., González-Hernández, A. I., Llorens, E., García-Agustín, P., Scalschi, L., & Vicedo, B. (2020). The Apoplast: A Key Player in Plant Survival. *Antioxidants*, 9(7), 604. https://dx.doi.org/10.3390/antiox9070604.

Ferrari, S., Galletti, R., Vairo, D., Cervone, F., & De Lorenzo, G. (2006). Anti-sense expression of the *Arabidopsis thaliana* AtPGIP1 gene reduces polygalacturonase-inhibiting protein accumulation and enhances susceptibility to Botrytis cinerea. *Molecular Plant-Microbe Interactions*, 19, 931–936.

Ferrari, S., Savatin, D. V., Sicilia, F., Gramegna, G., Cervone, F., & Lorenzo, G. D. (2013). Oligogalacturonides: Plant damage-associated molecular patterns and regulators of growth and development. *Frontiers in Plant Science*, 4, 49.

Ferro, M., Brugiere, S., Salvi, D., Seigneurin-Berny, D., Court, M., Moyet, L., ... Rolland, N. (2010). AT_CHLORO, a comprehensive chloroplast proteome database with subplastidial localization and curated information on envelope proteins. *Molecular & Cellular Proteomics*, 9, 1063–1084.

Foyer, C. H., Karpinska, B., & Krupinska, K. (2014). The functions of WHIRLY1 and REDOX-RESPONSIVE TRANSCRIPTION FACTOR 1 in cross tolerance responses in plants: A hypothesis. *Philosophical Transactions of the Royal Society of London, B:Biological Sciences*, 369, 20130226.

Galletti, R., Ferrari, S., & De Lorenzo, G. (2011). Arabidopsis MPK3 and MPK6 play different roles in basal and oligogalacturonide- or flagellin-induced resistance against *Botrytis cinerea*. *Plant Physiology*, 157, 804–814.

Galli, S., Jahn, O., Hitt, R., Hesse, D., Opitz, L., Plessmann, U., ... Jovin, T. M. (2009). A new paradigm for MAPK: Structural interactions of hERK1 with mitochondria in HeLa cells. *PLoS One*, 4, e7541.

Ge, C., Spanning, E., Glaser, E., & Wieslander, A. (2014). Import determinants of organelle-specific and dual targeting peptides of mitochondria and chloroplasts in *Arabidopsis thaliana*. *Molecular Plant*, 7, 121–136.

Gigli-Bisceglia, N., Savatin, D. V., Cervone, F., Engelsdorf, T., & De Lorenzo, G. (2018). Loss of the Arabidopsis protein kinases ANPs affects root cell wall composition, and triggers the cell wall damage syndrome. *Frontiers in Plant Science*, 8, 2234.

Gollan, P. J., Tikkanen, M., & Aro, E. M. (2015). Photosynthetic light reactions: Integral to chloroplast retrograde signalling. *Current Opinion in Plant Biology*, 27, 180–191.

Gómez-Gómez, L., & Boller, T. (2000). FLS2: An LRR receptor-like kinase involved in the perception of the bacterial elicitor flagellin in *Arabidopsis*. *Molecular Cell*, 5, 1003–1011.

Gonzalez Besteiro, M. A., & Ulm, R. (2013). Phosphorylation and stabilization of Arabidopsis MAP kinase phosphatase 1 in response to UV-B stress. *Journal of Biological Chemistry*, 288, 480–486.

Gravino, M., Locci, F., Tundo, S., Cervone, F., Savatin, D. V., & De Lorenzo, G. (2017). Immune responses induced by oligogalacturonides are differentially affected by AvrPto and loss of BAK1/BKK1 and PEPR1/PEPR2. *Molecular Plant Pathology*, 18, 582–595.

Guirimand, G., Guihur, A., Phillips, M. A., Oudin, A., Glevarec, G., Melin, C., ... Courdavault, V. (2012). A single gene encodes iso-pentenyl diphosphate isomerase isoforms targeted to plastids, mitochondria and peroxisomes in *Catharanthus roseus*. *Plant Molecular Biology*, 79, 443–459.

Gust, A. A., Pruitt, R., & Nürnberger, T. (2017). Sensing danger: Key to activating plant immunity. *Trends in Plant Science*, 22, 779–791.

Hanson, M. R., & Köhler, R. H. (2001). GFP imaging: methodology and application to investigate cellular compartmentation in plants. *Journal of Experimental Botany*, 52(356), 529–539. https://dx.doi.org/10.1093/jexbot/52.356.529.

Ishihara, H., Obata, T., Sulpice, R., Fernie, A. R., & Stitt, M. (2015). Quantifying protein synthesis and degradation in Arabidopsis by dynamic 13CO2 labeling and analysis of enrichment in individual amino acids in their free pools and in protein. *Plant Physiology*, 168, 74–93.

Jouannic, S., Hamal, A., Leprince, A. S., Tregear, J. W., Kreis, M., & Henry, Y. (1999). Plant MAP kinase kinase kinases structure, classification and evolution. *Gene*, 233, 1–11.

Karimi, M., Inze, D., & Depicker, A. (2002). GATEWAY vectors for agrobacterium-mediated plant transformation. *Trends in Plant Science*, 7, 193–195.

Kim, D. H., & Hwang, I. (2013). Direct targeting of proteins from the cytosol to organelles: The ER versus endosymbiotic organelles. *Traffic*, 14, 613–621.

Kleine, T., & Leister, D. (2016). Retrograde signaling: Organelles go networking. *Biochimica et Biophysica Acta*, 1857, 1313–1325.

Komis, G., Illes, P., Beck, M., & Samaj, J. (2011). Microtubules and mitogen-activated protein kinase signalling. *Current Opinion in Plant Biology*, 14, 650–657.

Komis, G., Šamajová, O., Ovečka, M., & Šamaj, J. (2018). Cell and Developmental Biology of Plant Mitogen-Activated Protein Kinases. *Annual Review of Plant Biology*, 69(1), 237–265. https://dx.doi.org/10.1146/annurev-arplant-042817-040314.

Kong, Q., Qu, N., Gao, M. H., Zhang, Z. B., Ding, X. J., Yang, F., … Zhang, Y. L. (2012). The MEKK1-MKK1/MKK2-MPK4 kinase cascade negatively regulates immunity mediated by a mitogen-activated protein kinase kinase kinase in Arabidopsis. *The Plant Cell*, 24, 2225–2236.

Kosugi, S., Hasebe, M., Tomita, M., & Yanagawa, H. (2009). Systematic identification of cell cycle-dependent yeast nucleocytoplasmic shuttling proteins by prediction of composite motifs. *Proceedings of the National Academy of Sciences, USA*, 106, 10171–10176.

Kovtun, Y., Chiu, W. L., Tena, G., & Sheen, J. (2000). Functional analysis of oxidative stress-activated mitogen-activated protein kinase cascade in plants. *Proceedings of the National Academy of Sciences, USA*, 97, 2940–2945.

Krysan, P. J., & Colcombet, J. (2018). Cellular complexity in MAPK signaling in plants: Questions and emerging tools to answer them. *Frontiers in Plant Science*, 9, 1674.

Krysan, P. J., Jester, P. J., Gottwald, J. R., & Sussman, M. R. (2002). An Arabidopsis mitogen-activated protein kinase kinase kinase gene family encodes essential positive regulators of cytokinesis. *The Plant Cell*, 14, 1109–1120.

Lampard, G., Wengier, D., & Bergmann, D. (2015). Correction. *The Plant Cell*, 27(7), 2073–2074. https://dx.doi.org/10.1105/tpc.15.00512.

Lee, J., Rudd, J. J., Macioszek, V. K., & Scheel, D. (2004). Dynamic changes in the localization of MAPK cascade components controlling pathogenesis-related (PR) gene expression during innate immunity in parsley. *Journal of Biological Chemistry*, 279, 22440–22448.

Li, J. F., Park, E., Von Arnim, A. G., & Nebenfuhr, A. (2009). The FAST technique: A simplified agrobacterium-based transformation method for transient gene expression analysis in seedlings of Arabidopsis and other plant species. *Plant Methods*, 5, 6.

Lian, K., Gao, F., Sun, T., van Wersch, R., Ao, K., Kong, Q., … Zhang, Y. (2018). MKK6 functions in two parallel MAP kinase cascades in immune signaling. *Plant Physiology*, 178, 1284–1295.

Littlejohn, G. R., Breen, S., Smirnoff, N., & Grant, M. (2020). Chloroplast immunity illuminated. *New Phytologist*. https://dx.doi.org/10.1111/nph.17076.

Liu, Y., Ren, D., Pike, S., Pallardy, S., Gassmann, W., & Zhang, S. (2007). Chloroplast-generated reactive oxygen species are involved in hypersensitive response-like cell death mediated by a mitogen-activated protein kinase cascade. *The Plant Journal*, 51, 941–954.

Livanos P., Galatis B., Apostolakos P. (2016). Deliberate ROS production and auxin synergistically trigger the asymmetrical division generating the subsidiary cells in Zea mays stomatal complexes. *Protoplasma*, 253(4), 1081–1099. https://dx.doi.org/10.1007/s00709-015-0866-6.

Mazars, C., Thuleau, P., Lamotte, O., & Bourque, S. (2010). Cross-talk between ROS and calcium in regulation of nuclear activities. *Molecular Plant*, 3, 706–718.

Meng, X., & Zhang, S. (2013). MAPK cascades in plant disease resistance signaling. *Annual Review of Phytopathology*, 51, 245–266.

Mhamdi, A., & Van Breusegem, F. (2018). Reactive oxygen species in plant development. *Development*, 145, dev164376.

Mitschke, J., Fuss, J., Blum, T., Hoglund, A., Reski, R., Kohlbacher, O., & Rensing, S. A. (2009). Prediction of dual protein targeting to plant organelles. *New Phytologist*, 183, 224–235.

Murashige, T., & Skoog, F. (1962). A Revised Medium for Rapid Growth and Bio Assays with Tobacco Tissue Cultures. *Physiologia Plantarum*, 15(3), 473–497. https://dx.doi.org/10.1111/j.1399-3054.1962.tb08052.x.

Nakagami, H., Soukupová, H., Schikora, A., Zárský, V., & Hirt, H. (2006). A Mitogen-activated Protein Kinase Kinase Kinase Mediates Reactive Oxygen Species Homeostasis inArabidopsis. *Journal of Biological Chemistry*, 281(50), 38697–38704. https://dx.doi.org/10.1074/jbc.m605293200.

Naseer, S., Lee, Y., Lapierre, C., Franke, R., Nawrath, C., & Geldner, N. (2012). Casparian strip diffusion barrier in Arabidopsis is made of a lignin polymer without suberin. *Proceedings of the National Academy of Sciences, USA*, 109, 10101–10106.

Nelson, B. K., Cai, X., & Nebenfuhr, A. (2007). A multicolored set of in vivo organelle markers for co-localization studies in Arabidopsis and other plants. *The Plant Journal*, 51, 1126–1136.

Nguyen Ba, A. N., Pogoutse, A., Provart, N., & Moses, A. M. (2009). NLStradamus: A simple hidden Markov model for nuclear localization signal prediction. *BMC Bioinformatics*, 10, 202.

Nie, S., Yue, H., Zhou, J., & Xing, D. (2015). Mitochondrial-derived reactive oxygen species play a vital role in the salicylic acid signaling pathway in *Arabidopsis thaliana*. *PLoS One*, 10, e0119853.

Nithianandarajah-Jones, G. N., Wilm, B., Goldring, C. E., Muller, J., & Cross, M. J. (2012). ERK5: Structure, regulation and function. *Cellular Signalling*, 24, 2187–2196.

Nomura, H., Komori, T., Uemura, S., Kanda, Y., Shimotani, K., Nakai, K., … Shiina, T. (2012). Chloroplast-mediated activation of plant immune signalling in Arabidopsis. *Nature Communications*, 3, 926.

Ovečka, M., Takáč, T., Komis, G., Vadovič, P., Bekešová, S., Doskočilová, A., … Šamaj, J. (2014). Salt-induced subcellular kinase relocation and seedling susceptibility caused by overexpression of Medicago SIMKK in Arabidopsis. *Journal of Experimental Botany*, 65(9), 2335–2350. https://dx.doi.org/10.1093/jxb/eru115.

Petrov, V. D., & Van Breusegem, F. (2012). Hydrogen peroxide-a central hub for information flow in plant cells. *AoB.Plants*, 2012, ls014.

Pfaffl, M. W. (2001). A new mathematical model for relative quantification in real-time RT-PCR. *Nucleic Acids Research*, 29, e45–e445.

Piques, M., Schulze, W. X., Hohne, M., Usadel, B., Gibon, Y., Rohwer, J., & Stitt, M. (2009). Ribosome and transcript copy numbers, polysome occupancy and enzyme dynamics in Arabidopsis. *Mol.Syst.Biol.*, 5, 314.

Puthiyaveetil, S., Kavanagh, T. A., Cain, P., Sullivan, J. A., Newell, C. A., Gray, J. C., … Allen, J. F. (2008). The ancestral symbiont sensor kinase CSK links photosynthesis with gene expression in chloroplasts. *Proceedings of the National Academy of Sciences, USA*, 105, 10061–10066.

Qi, J., Wang, J., Gong, Z., & Zhou, J. M. (2017). Apoplastic ROS signaling in plant immunity. *Current Opinion in Plant Biology*, 38, 92–100.

Radivojac, P., Vacic, V., Haynes, C., Cocklin, R. R., Mohan, A., Heyen, J. W., … Iakoucheva, L. M. (2010). Identification, analysis, and prediction of protein ubiquitination sites. *Proteins*, 78, 365–380.

Ren, Y., Li, Y., Jiang, Y., Wu, B., & Miao, Y. (2017). Phosphorylation of WHIRLY1 by CIPK14 shifts its localization and dual functions in Arabidopsis. *Molecular Plant*, 10, 749–763.

Saijo, Y., Loo, E. P., & Yasuda, S. (2018). Pattern recognition receptors and signaling in plant-microbe interactions. *The Plant Journal*, 93, 592–613.

Samajova, O., Komis, G., & Samaj, J. (2013). Emerging topics in the cell biology of mitogen-activated protein kinases. *Trends in Plant Science*, 18, 140–148.

Sasabe, M., & Machida, Y. (2012). Regulation of organization and function of microtubules by the mitogen-activated protein kinase cascade during plant cytokinesis. *Cytoskeleton (Hoboken.)*, *69*, 913–918.

Savatin, D. V., Gigli-Bisceglia, N., Marti, L., Fabbri, C., Cervone, F., & De Lorenzo, G. (2014a). The Arabidopsis NUCLEUS- AND PHRAGMOPLAST-LOCALIZED KINASE1-related protein kinases are required for elicitor-induced oxidative burst and immunity. *Plant Physiology*, *165*, 1188–1202.

Savatin, D. V., Gramegna, G., Modesti, V., & Cervone, F. (2014b). Wounding in the plant tissue: The defense of a dangerous passage. *Frontiers in Plant Science*, *5*, 470.

Schneider-Poetsch, T., Ju, J., Eyler, D. E., Dang, Y., Bhat, S., Merrick, W. C., … Liu, J. O., (2010). Inhibition of eukaryotic translation elongation by cycloheximide and lactimidomycin. *Nature Chemical Biology*, *6*(3), 209–217. https://dx.doi.org/10.1038/nchembio.304.

Schwab, R., Ossowski, S., Riester, M., Warthmann, N., & Weigel, D. (2006). Highly Specific Gene Silencing by Artificial MicroRNAs in Arabidopsis. *The Plant Cell*, *18*(5), 1121–1133. https://dx.doi.org/10.1105/tpc.105.039834.

Schwessinger, B., & Ronald, P. C. (2012). Plant innate immunity: Perception of conserved microbial signatures. *Annual Review of Plant Biology*, *63*, 451–482.

Shapiguzov, A., Vainonen, J. P., Wrzaczek, M., & Kangasjarvi, J. (2012). ROS-talk - how the apoplast, the chloroplast, and the nucleus get the message through. *Frontiers in Plant Science*, *3*, 292.

Sies, H., & Jones, D. P. (2020). Reactive oxygen species (ROS) as pleiotropic physiological signalling agents. *Nature Reviews: Molecular Cell Biology*, *21*, 363–383.

Su, S. H., Bush, S. M., Zaman, N., Stecker, K., Sussman, M. R., & Krysan, P. (2013). Deletion of a tandem gene family in Arabidopsis: Increased MEKK2 abundance triggers autoimmunity when the MEKK1-MKK1/2-MPK4 signaling Cascade is disrupted. *The Plant Cell*, *25*, 1895–1910.

Suarez Rodriguez, M. C., Petersen, M., & Mundy, J. (2010). Mitogen-activated protein kinase signaling in plants. *Annual Review of Plant Biology*, *61*, 621–649.

Takahashi, Y., Soyano, T., Kosetsu, K., Sasabe, M., & Machida, Y. (2010). HINKEL kinesin, ANP MAPKKKs and MKK6/ANQ MAPKK, which phosphorylates and activates MPK4 MAPK, constitute a pathway that is required for cytokinesis in *Arabidopsis thaliana*. *Plant and Cell Physiology*, *51*, 1766–1776.

Tardif, M., Atteia, A., Specht, M., Cogne, G., Rolland, N., Brugiere, S., … Cournac, L. (2012). PredAlgo: A new subcellular localization prediction tool dedicated to green algae. *Molecular Biology and Evolution*, *29*, 3625–3639.

Tejos, R. I., Mercado, A. V., & Meisel, L. A. (2010). Analysis of chlorophyll fluorescence reveals stage specific patterns of chloroplast-containing cells during Arabidopsis embryogenesis. *Biological Research*, *43*, 99–111.

Wainstein, E., & Seger, R. (2016). The dynamic subcellular localization of ERK: Mechanisms of translocation and role in various organelles. *Current Opinion in Cell Biology*, *39*, 15–20.

Wang, Y., Selinski, J., Mao, C., Zhu, Y., Berkowitz, O., & Whelan, J. (2020). Linking mitochondrial and chloroplast retrograde signalling in plants. *Philosophical Transactions of the Royal Society of London, B:Biological Sciences*, *375*, 20190410.

Waszczak, C., Carmody, M., & Kangasjarvi, J. (2018). Reactive oxygen species in plant signaling. *Annual Review of Plant Biology*, *69*, 209–236.

Xing, Y., Jia, W., & Zhang, J. (2009). AtMKK1 and AtMPK6 are involved in abscisic acid and sugar signaling in Arabidopsis seed germination. *Plant Molecular Biology*, *70*, 725–736.

Xu, J., & Zhang, S. (2015). Mitogen-activated protein kinase cascades in signaling plant growth and development. *Trends in Plant Science*, *20*, 56–64.

Yamasaki, H., Shimoji, H., Ohshiro, Y., & Sakihama, Y. (2001). Inhibitory effects of nitric oxide on oxidative phosphorylation in plant mitochondria. *Nitric Oxide*, *5*, 261–270.

Zhang, M., Su, J., Zhang, Y., Xu, J., & Zhang, S. (2018). Conveying endogenous and exogenous signals: MAPK cascades in plant growth and defense. *Current Opinion in Plant Biology*, *45*, 1–10.

Zhang, Z., Liu, Y., Huang, H., Gao, M., Wu, D., Kong, Q., & Zhang, Y. (2017). The NLR protein SUMM2 senses the disruption of an immune signaling MAP kinase cascade via CRCK3. *EMBO Reports*, *18*, 292–302.

Zipfel, C., Kunze, G., Chinchilla, D., Caniard, A., Jones, J. D. G., Boller, T., & Felix, G. (2006). Perception of the bacterial PAMP EF-Tu by the receptor EFR restricts *Agrobacterium*-mediated transformation. *Cell*, *125*, 749–760.

SUPPORTING INFORMATION

Additional supporting information may be found online in the Supporting Information section at the end of this article.